Gaia-based Isochronal, Kinematic, and Spatial Analysis of the ϵ Cha Association

D. Annie Dickson-Vandervelde[1,2], Emily C. Wilson[1,3] , and Joel H. Kastner[1,2,4]

[1] School of Physics and Astronomy, Rochester Institute of Technology, Rochester NY 14623, USA; dad1197@rit.edu
[2] Laboratory for Multiwavelength Astrophysics, Rochester Institute of Technology, USA
[3] Center for Computational Relativity and Gravitation, Rochester Institute of Technology, USA
[4] Center for Imaging Science, Rochester Institute of Technology, USA; jhk@cis.rit.edu

Received 2020 July 21; revised 2020 December 2; accepted 2020 December 3; published 2021 January 28

Abstract

The precise parallax, proper motion, and photometric measurements contained in Gaia Data Release 2 (DR2) offer the opportunity to reexamine the membership and ages of nearby young moving groups (NYMGs), i.e., loose groups of stars of age $\lesssim$100 Myr in the solar vicinity. Here, we analyze the available DR2 data for members and candidate members of the ϵ Cha Association (ϵCA) which, at an estimated age of $\sim$3–5 Myr, has previously been identified as among the youngest NYMGs. The several dozen confirmed members of ϵCA include MP Mus and T Cha, two of the nearest stars of roughly solar mass that are known to host primordial protoplanetary disks, and the Herbig Ae/Be star HD 104237A. We have used Gaia DR2 data to ascertain the Galactic positions and kinematics and color–magnitude diagram positions of ϵCA members and candidates so as to reassess their membership status and thereby refine estimates of the distance, age, multiplicity, and disk fraction of the group. Our analysis yields 36 bona fide ϵCA members, as well as 20 provisional members, including 3 new members identified here as comoving companions to previously known ϵCA stars. We determine a mean distance to ϵCA of 101.0 $\pm$ 4.6 pc and confirm that, at an age of 5^{+3}_{-2} Myr, ϵCA represents the youngest stellar group within $\sim$100 pc of Earth. We identify several new photometric binary candidates, bringing the overall multiplicity fraction (MF) of ϵCA to 40%, intermediate between the MFs of young T associations and the field.

Unified Astronomy Thesaurus concepts: Stellar associations (1582); Pre-main sequence stars (1290)

1. Introduction

Nearby young moving groups (NYMGs) serve as laboratories for the study of stars and their planetary offspring during their first stages of development, i.e., over the first tens of Myr after these young stars and planets have emerged from their birth clouds (Kastner et al. 2019). The age range spanned by coeval NYMGs (a few Myr to several ×100 Myr) provides unique opportunities to study stellar properties over a range of masses and temperatures at specific snapshots of pre-main sequence (pre-MS) and young MS evolution. Thanks to the proximity (<120 pc) of NYMGs, it is possible to observe and characterize an entire stellar population, down to the diminutive brown dwarfs (e.g., Schneider et al. 2019; Phillips et al. 2020) and even massive planets (e.g., Gagné et al. 2018b). The younger NYMGs (ages <25 Myr) feature Sun-like stars orbited by gas-rich circumstellar disks that are likely sites of ongoing planet formation (e.g., Sacco et al. 2014), while dusty debris disks are found among groups at more advanced ages (e.g., Zuckerman et al. 2019).

The precise astrometric and photometric data flowing from the Gaia Space Astrometry mission (Gaia Collaboration et al. 2016, 2018) is particularly useful to the study of NYMGs. Gaia Data Release 1 and the subsequent Gaia Data Release 2 (hereafter DR2) have resulted in a leap in our understanding of the membership of previously known NYMGs and, hence, their fundamental properties, such as ages, mass distributions, internal kinematics, and stellar multiplicity statistics (e.g., Gagné & Faherty 2018; Wright & Mamajek 2018; Lee & Song 2019). Gaia DR2 data have also led to the identification of previously unknown NYMGs (e.g., Gagné et al. 2018a).

Here, we present an analysis of Gaia DR2 data for the ϵ Chamaeleontis Association (hereafter ϵCA). At an estimated age of 3–5 Myr (Murphy et al. 2013, henceforth M+13), ϵCA is the

youngest NYMG within $\sim$100 pc of Earth (Kastner et al. 2019 and references therein). Its relative youth and consequent large disk frequency (29%, M+13)—combined with its position well in the foreground of the Cha star formation complex (see Figure 2 of M+13)—make it a key NYMG for purposes of studying planet formation and pre-MS stellar evolution, without the complication of pervasive ambient or intervening molecular cloud material.

The identification and study of stars belonging to ϵCA began in association with the study of the neighboring η Cha cluster (Mamajek et al. 2000). Chandra X-ray Observatory observations of the Herbig Ae/Be star HD 104237A ϵCA led to further characterization of the group and discovery of new members (Feigelson et al. 2003). HD 104237A has a close, T Tauri-type companion (HD 104237B), both of which are orbited by a CO-rich circumbinary disk (Hales et al. 2014). An additional three stars are thought to be part of the HD 104237 system, two of which form another close binary (HD 104237D+E); HD 104237D shows evidence of accreting plasma (Testa et al. 2008).

In addition to HD 104237A, the members of ϵCA include two stars with gas-rich circumstellar disks, MP Mus and T Cha; these stars represent two of only four known examples of solar-mass stars with protoplanetary disks that lie within $\sim$100 pc of Earth (Kastner et al. 2010; Sacco et al. 2014). Among these four, the disk orbiting MP Mus—a single, 1.2 $M_\odot$ star lying a mere 98 pc from Earth—may be most closely analogous to the solar nebula. Meanwhile, the T Cha disk is the only nearby transition disk that is viewed at a high inclination (73°) and furthermore displays evidence for an embedded planet (Hendler et al. 2018).

The most recent comprehensive study of the membership of ϵCA (M+13) was reliant on pre-Gaia stellar kinematics and photometry. With the benefit of Gaia DR2 data, we have

revisited and refined the membership, kinematics, and color–magnitude distribution of ϵCA, with the primary goal of firmly establishing its position along the NYMG age sequence. We have also reexamined the multiplicity of ϵCA members and the detailed spatial distribution of disk-bearing stars in the group. In Section 2, we discuss the sample selection and flags and caveats of the available Gaia DR2 data. In Section 3, we describe our methods, including determination of an empirical isochrone and kinematics for the ϵCA. In Section 4, we present the results from this analysis. In Section 5, we discuss the implications of these results, including the age of ϵCA relative to other young NYMGs.

2. Sample Selection

Table 1 lists all (65) stars we considered for ϵCA membership for which Gaia DR2 data is available. The majority of these ϵCA candidates were drawn from M+13. Those authors gathered all proposed members of ϵCA from the previous literature (52 in total) and assessed membership via their (pre-Gaia) proper motions and their spectral properties (such as Li absorption-line equivalent widths and infrared excesses). The set of 35 stars initially considered here as bona fide ϵCA members then consists of M+13's "confirmed members" (M+13 Table 7). Ultimately, we also considered the 6 "provisional members" and 11 "rejected stars" from the M+13 study (Section 4.1) as well as 15 stars from Gagné & Faherty (2018, henceforth GF18) that GF18 designated as potential ϵCA members (Section 4.1.4).

We searched the Gaia archive for DR2 counterparts to these 67 stars from the M+13 and GF18 studies, using a 0″25 search radius centered at the position listed in M+13. Unique DR2 counterparts were identified for all stars listed in Table 1, comprising a total of 65 of the 67 stars searched, though not all of these counterparts had parallaxes and colors. All Gaia counterparts met or exceeded the minimum number of Gaia visibility periods ($n_{vis} > 5$) recommended by Lindegren et al. (2018).

To assess the quality of the Gaia data for individual stars, we applied three metrics: the renormalized unit weight error (RUWE; Lindegren 2018), astrometric excess noise, and photometric excess (Gaia Collaboration et al. 2018). The astrometric unit weight error (UWE), in its renormalized form (RUWE), is useful to determine when data are potentially unreliable based on Gaia measurement uncertainties alone. Following Lindegren (2018), we flag data with RUWE > 1.4. Note that this RUWE threshold is implicitly based on a star's $G_{B_p} - G_{R_p}$ color, whereas the color–magnitude diagram analysis carried out here (Section 3.1) uses Gaia $G - G_{R_p}$ colors. We also utilized `astrometric_excess_noise` to assess the quality of the astrometric data, flagging those stars with `astrometric_excess_noise` $> 0.1 \times \pi$ as having potentially large parallax uncertainties. We used Gaia's `phot_bp_rp_excess_factor`, E, to flag stars that did not satisfy $1.0 + 0.015(G_{B_p} - G_{R_p})^2 < E < 1.3 + 0.06(G_{B_p} - G_{R_p})^2$. As discussed in Gaia Collaboration et al. (2018), stars that fall outside of this range of $G_{B_p} - G_{R_p}$ have colors that may not be trustworthy.

The RUWE values for all 65 stars are listed in Table 1. The results of the astrometric excess noise and photometric excess tests are also noted in Table 1. Two stars, T Cha and HD 104237E, fail the `phot_bp_rp_excess_factor` test. In Figure 1, we display the Gaia DR2 color–magnitude diagram (CMD) positions of the 30 (of 35) bona fide M+13 ϵCA members

that have viable DR2 parallaxes and photometry (see Section 3.1), with the results of the preceding data-flagging exercise indicated.

3. Analysis

3.1. Empirical Single-star Isochrone

To ascertain the empirical isochrone defined by single-star members of NYMGs like ϵCA, we have developed the single-star locus fitting routine (SLFR; D. A. Dickson-Vandervelde et al. 2020, in preparation). The SLFR utilizes a recursive method to fit a polynomial to the color–magnitude diagram (CMD) of a set of NYMG members, identifying and rejecting outliers at each iteration. Between iterations, any star with a magnitude greater than 2σ is rejected before refitting the polynomial. The final result is a polynomial that represents the best fit to the single-star locus of the group across well-sampled regions of color–magnitude space, as well as a list of candidate photometric binaries, i.e., stars that lie significantly above, but within ∼0.75 mag of, the single-star locus. The resulting best-fit polynomial then effectively represents the group's empirical single-star isochrone.

Only 32 of the 33 bona fide members of ϵCA listed in Table 1 have the DR2 parallaxes and photometry necessary for SLFR analysis; we further excluded two stars whose parallaxes appear incompatible with ϵCA membership (see Section 4.1.2). Figure 1 illustrates the results of the SLFR method as applied to the remaining 30 stars. The SLFR-generated empirical isochrone (polynomial) is only well fit where there is a good sampling of stars in color–magnitude space and is particularly unreliable (and is therefore not plotted) in the bluest region of the CMD ($G - G_{RP} < 0.5$). We found a fourth-order polynomial to be sufficient to match the color–magnitude data without introducing artifacts in poorly sampled regions. The final polynomial is given by $G = 1.28c^4 + 8.44c^3 - 28.9c^2 + 33.17c + 7.18$, where G is the absolute G magnitude and c is the $G - G_{RP}$ color. This fit provided an rms in G of 0.61 mag. Hereafter, we refer to this polynomial as the empirical (5 Myr) isochrone.

The empirical isochrone is evidently a better match to the ϵCA color–magnitude data than any of the theoretical isochrones (from Tognelli et al. 2018) plotted in Figure 1. While the 5 and 8 Myr theoretical isochrones follow the SLFR-generated empirical isochrone in the blue CMD regions (i.e., $G - G_{RP}$ in the range 0.2–0.8), both of these isochrones fall below the NYMG distribution for redder colors ($G - G_{RP} > 0.8$). This general behavior, in which theoretical isochrones fall under the single-star loci of NYMGs in Gaia-based CMDs, has been well documented in the recent literature (e.g., Gagné et al. 2018a). Nonetheless, it is apparent that the 5 Myr isochrone appears to be the best overall match to the SLFR-generated empirical isochrone. We further discuss the implications of the comparison between empirical and theoretical isochrones for the age of the ϵCA in Section 5.3.

The SLFR polynomial fitting exercise yields five photometric binary candidates among the 30 bona fide M+13 ϵCA members plotted in Figure 1. Of note, the majority of these binary-star candidates have high RUWE. This is consistent with the results of Belokurov et al. (2020), who found that stars along the binary-star locus within all Gaia data show higher RUWEs than stars along the single-star locus. This correlation is likely a result of marginally resolved, close binaries yielding low-precision astrometric solutions. The SLFR method also flagged two clear CMD outliers among the 32 bona fide

Table 1
Gaia Data and RVs for Candidate εCA Members

Name[a]	R.A. (J2015.5) (deg)	Decl. (J2015.5) (deg)	π (mas)	σ	G (mag)	σ	$G - R_P$ (mag)	σ	PMRA (mas yr^{-1})	σ	PMDec (mas yr^{-1})	σ	RV (km s^{-1})	σ	RUWE[b]	RV ref[c]
HD 8279*	142.0874	−78.2597	8.504	0.025	8.92760	0.00038	0.3737	0.0025	−28.211	0.043	20.350	0.046	12.76	0.2	1.05	2
CP−68 1388[†]	164.4553	−69.2333	8.592	0.029	10.0229	0.0024	0.6763	0.0070	−34.842	0.051	3.552	0.044	15.9	1.0	0.93	12
VW Cha*	167.0058	−77.7079	⋯	⋯	12.187	0.020	1.425	0.018	⋯	⋯	⋯	⋯	⋯	⋯	⋯	
TYC 9414-191-1[‡]	169.1200	−78.4224	1.564	0.022	10.523674	0.00025	0.86718	0.00067	−38.372	0.040	2.460	0.033	⋯	⋯	0.91	⋯
2MASS J11183572−7935548[†]	169.6478	−79.5986	10.57	0.15	13.8687	0.0027	1.3726	0.0043	−41.76	0.26	4.98	0.24	19.3	1.6	3.35[+]	8
RX J1123.2−7924*	170.7311	−79.4123	9.379	0.021	12.8674	0.0016	1.0036	0.0041	−31.670	0.040	−17.443	0.038	2.7	2.9	1.14	8
HIP 55746*	171.3217	−84.9545	11.077	0.138	7.53435	0.00044	0.3524	0.0021	−46.19	0.16	11.92	0.16	20.9	1.2	1.46	3
2MASS J11334926−7618399*	173.4550	−76.3111	5.410	0.060	15.56704	0.00081	1.3373	0.0010	−22.41	0.11	−0.561	0.087	⋯	⋯	1.07	⋯
RX J1137.4−7648*	174.3794	−76.7997	11.988	0.021	13.52653	0.00079	1.0494	0.0022	−60.544	0.041	−8.935	0.032	14.0	5.0	1.16	8
2MASS J11404967−7459394[†]	175.2063	−74.9942	10.397	0.069	16.4291	0.0018	1.4466	0.0044	−42.74	0.13	−2.28	0.10	10.3	1.0	0.94	8
2MASS J11411722−7315369[#]	175.3211	−73.2602	10.416	0.052	15.47804	0.00084	1.3229	0.0024	−42.047	0.093	5.672	0.082	⋯	⋯	1.07	⋯
TYC 9238-612-1*	175.3646	−73.7841	6.124	0.021	10.5976	0.0012	0.5663	0.0035	−35.747	0.041	10.938	0.036	⋯	⋯	1.33	⋯
2MASS J11432669−7804454[†]	175.8603	−78.0793	5.54	0.56	14.8931	0.0072	1.321	0.022	−43.98	0.92	−6.52	0.75	15.6	1	10.51[+]	8
2MASS J11432968−7418377[#]	175.8729	−74.3105	10.063	0.039	14.17633	0.00066	1.2213	0.0022	−40.621	0.073	−3.026	0.067	⋯	⋯	1.19	⋯
RX J1147.7−7842[†]	176.9496	−78.698	9.894	0.039	12.3523	0.0012	1.1840	0.0028	−41.660	0.075	−4.265	0.065	16.1	0.9	1.28	8
RX J1149.8−7850[†]	177.3818	−78.8503	9.918	0.025	11.9324	0.0043	1.028	0.015	−41.876	0.047	−4.265	0.040	13.4	1.3	1.19	8
RX J1150.4−7704*	177.6171	−77.0773	6.551	0.031	11.5250	0.0016	0.7773	0.0042	−42.744	0.054	−11.047	0.040	⋯	⋯	1.26	⋯
RX J1150.9−7411[†]	177.6868	−74.1871	10.63	0.18	13.4567	0.0050	1.324	0.012	−39.50	0.32	−8.08	0.29	15.0	1.2	6.01[+]	8
2MASS J11550485−7919108[†]	178.7692	−79.3198	9.886	0.058	14.8180	0.0017	1.3502	0.0053	−41.18	0.13	−4.336	0.086	⋯	⋯	1.08	⋯
T Cha[†]	179.3054	−79.3588	9.122	0.083	12.97	0.11	1.61	0.35	−42.00	0.12	−9.245	0.080	6–30	⋯	0.91	2,5,10
RX J1158.5−7754B[†]	179.6109	−77.9126	9.662	0.035	13.2023	0.0027	1.1713	0.0081	−39.573	0.064	−5.686	0.060	13.0	2.0	1.22	11
RX J1158.5−7754A[†]	179.6165	−77.9083	9.518	0.035	9.9798	0.0011	0.7888	0.0033	−39.660	0.063	−12.844	0.070	14.02	1.82	1.66	2,8,12
HD 104036[†]	179.646	−77.8254	9.566	0.038	6.69296	0.00053	0.1646	0.0041	−41.286	0.065	−7.762	0.073	12.6	0.5	1.23	3
CXOU J115908.2−781232[‡]	179.7824	−78.2089	9.425	0.062	15.2563	0.00063	1.3139	0.0022	−38.62	0.14	−5.181	0.091	15.1	0.2	1.24	8
ε Cha AB[†]	179.9056	−78.2219	⋯	⋯	4.7816	0.0080	−0.1505	0.0086	⋯	⋯	⋯	⋯	13	3.7	⋯	11
RX J1159.7−7601[†]	179.9254	−76.024	10.025	0.023	10.8095	0.0023	0.7694	0.0058	−41.025	0.043	−6.190	0.038	13.0	3.7	0.96	2,8
2MASS J12000269−7444068[#]	180.0105	−74.7352	10.067	0.049	14.3241	0.0011	1.2431	0.0028	−42.047	0.079	−5.699	0.071	⋯	⋯	1.24	⋯
HD 104237A[†]	180.0204	−78.193	9.226	0.058	6.5427	0.0018	0.2213	0.0074	−39.31	0.11	−6.212	0.083	13.52	0.39	1.55	4
HD 104237D[†]	180.0336	−78.1943	9.885	0.061	13.0206	0.0015	1.1981	0.0065	−38.87	0.13	−3.195	0.098	⋯	⋯	1.53	⋯
HD 104237E[†]	180.0379	−78.1951	9.796	0.034	11.838	0.028	1.16	0.11	−42.907	0.074	−4.418	0.051	⋯	⋯	1.54	⋯
2MASS J12005517−7820296[†]	180.2291	−78.3415	9.713	0.082	15.5826	0.0012	1.4005	0.0040	−40.59	0.14	−4.96	0.12	10.7	1.3	1.17	8

3

Table 1
(Continued)

Name[a]	R.A. (J2015.5) (deg)	Decl. (J2015.5) (deg)	π (mas)	σ	G (mag)	σ	$G - R_P$ (mag)	σ	PMRA (mas yr^{-1})	σ	PMDec (mas yr^{-1})	σ	RV (km s^{-1})	σ	RUWE[b]	RV ref[c]
HD 104467[†]	180.412	−78.9881	10.14	0.17	8.4285	0.0022	0.5145	0.0059	−41.11	0.26	−5.41	0.26	12.81	0.96	5.17	2
2MASS J12014343−7835472[†]	180.4302	−78.5965	9.53	0.11	17.115	0.021	1.166	0.069	−41.32	0.19	−6.33	0.14	20.0	0.6	1.28	8
USNO-B 120144.7−781926[†]	180.4343	−78.3241	9.819	0.063	15.2758	0.0076	1.372	0.020	−41.43	0.11	−6.105	0.088	14.9	1.1	1.08	8
CXOU J120152.8−781840[†]	180.4681	−78.3115	9.735	0.068	14.9821	0.0012	1.3319	0.0026	−40.59	0.12	−6.88	0.10	16.5	1.1	1.14	8
RX J1202.1−7853[†]	180.5145	−78.8837	10.011	0.046	11.5100	0.0030	1.0059	0.0088	−45.122	0.081	−4.124	0.069	17.1	0.2	1.63	5
RX J1202.8−7718[‡]	180.7269	−77.3106	9.606	0.035	13.3749	0.0026	1.1762	0.0080	−39.625	0.072	−6.044	0.059	14.4	0.6	1.21	7
RX J1204.6−7731[†]	181.1498	−77.5263	9.922	0.034	12.5714	0.0018	1.1513	0.0053	−41.364	0.056	−6.397	0.052	10.4	2.0	1.20	6
TYC 9420-676-1[*]	181.2384	−79.5346	3.700	0.080	10.23947	0.00063	0.4443	0.0016	−38.16	0.16	−1.00	0.18	⋯	⋯	2.95	⋯
HD 105234[‡]	181.7721	−78.7412	9.566	0.035	7.41947	0.00041	0.2247	0.0028	−40.971	0.058	−9.41	0.057	⋯	⋯	1.15	⋯
2MASS J12074597−7816064[*]	181.9407	−78.2685	9.454	0.058	14.55144	0.00073	1.2293	0.0021	−38.424	0.091	−6.319	0.077	15.2	1.9	1.33	8
RX J1207.7−7953[†]	181.9501	−79.8785	10.016	0.030	13.3403	0.0022	1.1860	0.0057	−42.058	0.056	−7.113	0.052	15.0	0.7	1.12	8
HIP 59243[‡]	182.2811	−78.7813	10.019	0.033	6.79373	0.00043	0.1889	0.0034	−43.364	0.062	−7.619	0.06	⋯	⋯	1.10	⋯
HD 105923[†]	182.9084	−71.1767	9.400	0.036	8.83653	0.00083	0.5367	0.0035	−38.721	0.062	−7.423	0.051	14.34	1.06	0.87	1,2,12
RX J1216.8−7753[†]	184.1906	−77.8927	9.820	0.039	12.9206	0.0037	1.132	0.010	−39.825	0.072	−9.074	0.072	14.0	2.0	1.17	6
RX J1219.7−7403[†]	184.9315	−74.0659	9.865	0.027	12.1400	0.0016	1.0187	0.0042	−40.323	0.043	−9.256	0.039	13.86	1.89	0.96	2
RX J1220.4−7407[†]	185.0901	−74.1277	6.71	0.70	11.9406	0.0020	1.0706	0.0050	−40.9	1.2	−4.1	1.4	12.3	0.4	38.28[+]	6
2MASS J12203396−7135188[#]	185.1411	−71.5886	10.773	0.057	13.21947	0.00084	1.2486	0.0019	−42.573	0.096	−8.571	0.070	⋯	⋯	1.28	⋯
2MASS J12203619−7353027[#]	185.1502	−73.8842	10.007	0.035	13.1409	0.0010	1.1424	0.0024	−40.621	0.069	−9.326	0.050	⋯	⋯	1.12	⋯
2MASS J12210499−7116493[†]	185.2703	−71.2804	10.055	0.024	11.2032	0.0028	0.8874	0.0079	−40.416	0.043	−9.647	0.034	11.44	2.53	1.02	9
2MASS J12220068−7001041[#]	185.5022	−70.0178	10.008	0.047	14.0236	0.0011	1.2371	0.0045	−41.229	0.096	−10.474	0.063	⋯	⋯	1.23	⋯
2MASS J12222238−7137040[#]	185.5926	−71.6178	10.516	0.027	12.5299	0.0081	1.105	0.023	−41.843	0.044	−9.962	0.043	⋯	⋯	1.06	⋯
2MASS J12224862−7410203[#]	185.702	−74.1724	10.605	0.089	16.1751	0.0024	1.4774	0.0068	−42.57	0.15	−9.27	0.13	⋯	⋯	1.18	⋯
2MASS J12255824−7551116[#]	186.4921	−75.8533	10.049	0.065	15.36554	0.00074	1.3318	0.0026	−41.23	0.11	−10.46	0.10	⋯	⋯	1.20	⋯
2MASS J12324805−7654237[#]	188.1995	−76.9067	11.69	0.91	12.8346	0.0012	1.1960	0.0033	−41.84	1.67	−13.49	1.32	⋯	⋯	36.83[+]	⋯
2MASS J12332483−6848553[#]	188.3531	−68.8154	10.061	0.086	15.7118	0.0012	1.3676	0.0039	−41.43	0.13	−12.51	0.11	⋯	⋯	1.16	⋯
2MASS J12351540−7043079[#]	188.8135	−70.7189	10.705	0.066	15.70148	0.00068	1.3844	0.0026	−43.72	0.11	−12.639	0.094	⋯	⋯	1.03	⋯
RX J1239.4−7502[†]	189.838	−75.0443	9.646	0.027	9.9751	0.0017	0.6679	0.0048	−38.214	0.044	−12.368	0.042	13.62	2.8	0.97	9

Table 1
(Continued)

Name[a]	R.A. (J2015.5) (deg)	Decl. (J2015.5) (deg)	π (mas)	σ	G (mag)	σ	$G - R_P$ (mag)	σ	PMRA (mas yr^{-1})	σ	PMDec (mas yr^{-1})	σ	RV (km s^{-1})	σ	RUWE[b]	RV ref[c]
2MASS J12421315−6943484[#]	190.5543	−69.7302	10.062	0.083	15.1444	0.0011	1.3551	0.0039	−39.50	0.14	−12.77	0.10	⋯	⋯	1.24	⋯
RX J1243.1−7458[*]	190.7219	−74.98	7.99	0.37	13.7652	0.0044	1.186	0.011	−17.25	0.66	−2.63	0.53	13.5	7.0	10.71[+]	8
2MASS J12425584−7034207[#]	190.7321	−70.5725	10.062	0.078	15.97496	0.00098	1.4049	0.0031	−40.47	0.12	−13.20	0.12	⋯	⋯	0.99	⋯
2MASS J12473611−7031135[#]	191.9000	−70.5206	10.012	0.031	13.26920	0.00065	1.1498	0.0016	−40.249	0.048	−14.241	0.045	⋯	⋯	1.12	⋯
CD-69 1055[†]	194.6061	−70.4804	10.549	0.029	9.6062	0.0027	0.6388	0.0076	−41.001	0.047	−16.459	0.045	11.18	1.67	1.01	1,2,8
CM Cha[‡]	195.5560	−76.6328	5.152	0.024	12.5599	0.0043	1.001	0.012	−20.990	0.040	−9.144	0.041	⋯	⋯	1.15	⋯
MP Mus[†]	200.531	−69.6368	10.115	0.031	9.9521	0.0030	0.7207	0.0087	−38.289	0.044	−20.204	0.045	11.6	0.2	0.98	12

Notes.

[a] M+13 bona fide members are indicated by †, M+13 provisional members are indicated by ‡, M+13 rejected members are indicated by *, and GF18 members are indicated by #.

[b] Values marked with + have high astrometric excess noise.

[c] References for radial velocities: (1) Desidera et al. (2015), (2) Gaia Collaboration et al. (2018), (3) Gontcharov (2006), (4) Grady et al. (2004), (5) Guenther et al. (2007), (6) Lopez Martí et al. (2013), (7) Malo et al. (2014), (8) Murphy et al. (2013), (9) Kordopatis et al. (2013), (10) Schisano et al. (2009), (11) Terranegra et al. (1999), (12) Torres et al. (2006).
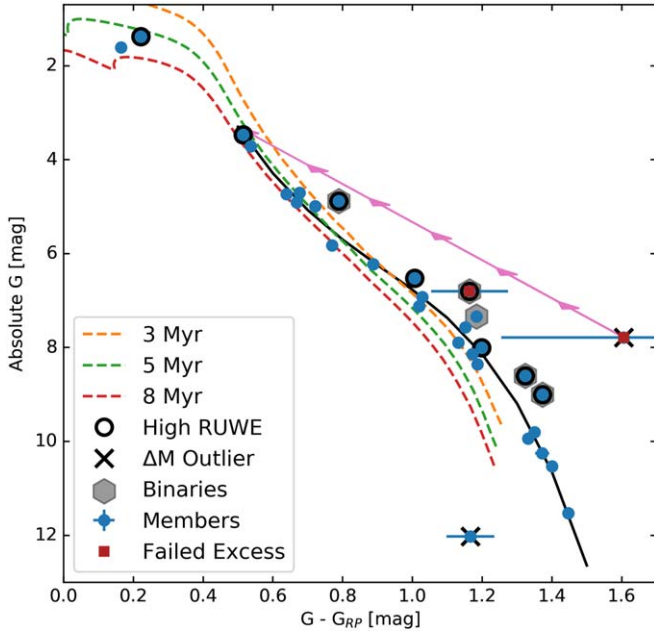
Figure 1. Gaia DR2 color–magnitude diagram (CMD) for the 30 M+13 bona fide members (blue circles) included in empirical single-star locus fitting (SLFR) analysis (Section 3.1). The best-fit empirical isochrone obtained from the SLFR method is represented by the black curve. Three theoretical isochrones (Tognelli et al. 2018) for ages of 3, 5, and 8 Myr (orange, green, and red dashed lines, respectively) are also overlaid on the data. Stars with high RUWE values (low-accuracy astrometry) are marked with black, open circles; stars failing the color excess factor test (bad photometry) are marked with red squares; and stars that are outliers in magnitude offset are marked with crosses. Five stars identified as candidate photometric binaries (via the empirical single-star isochrone fitting) are denoted by gray hexagons. Errors are displayed as horizontal and vertical bars in blue; where no error bar is seen, the errors are smaller than the symbols. The pink line (with arrows) represents the reddening vector inferred for T Cha (the red square and cross at $G - G_{RP} \sim 1.6$), i.e., $E(G - G_{RP}) = 1.1$ mag and $A_G = 4.5$ mag (see Section 4.1.3).

members, T Cha and 2MASS J12014343–7835472, both of which are discussed in Section 4.1.3.

3.2. Kinematic Analysis

We calculated the heliocentric space motions and positions of the (35) stars considered as ϵCA members by M+13 (Section 2) for which proper motions, parallaxes, and radial velocities (RVs) are available (see Table 1). Gaia DR2 provides RVs for eight stars, and the remaining (majority) of the RVs come from M+13 and other RV surveys in the literature (see footnote b of Table 1). Heliocentric velocities (*UVW*) and positions (*XYZ*) were calculated using code from BANYAN Σ (Gagné et al. 2018c). In cases where a star had multiple RV measurements, we adopt the mean RV to calculate *UVW*, except in the case of T Cha (see Section 4.1.3). The resulting *UVW* were used to reevaluate ϵCA membership (Section 4.1).

4. Results

4.1. Membership

4.1.1. Kinematic and Photometric Inclusion/Rejection Parameters and Criteria

We employed two quantitative criteria, kinematic offset ($K_{\rm kin}$) and magnitude offset (ΔM), to help assess ϵCA membership. These two metrics, listed in Table 2, correspond to those defined in M+13. Specifically, the kinematic offset is

defined as

$$K_{\rm kin} = \sqrt{(U - U_0)^2 + (V - V_0)^2 + (W - W_0)^2}, \quad (1)$$

where (U_0, V_0, W_0) is the mean space motion for ϵCA as calculated from the 30 bona fide M+13 members used for the SLFR analysis (Section 3.1). We defined ΔM as

$$\Delta M = M'(c) - M, \quad (2)$$

where c is the color of the star, $M'(c)$ is the absolute magnitude of the empirical isochrone at the star's color, and M is the measured absolute G magnitude of the star. Outliers in ΔM are those with $|\Delta M| \geqslant 2\sigma_{\Delta M}$ and in $K_{\rm kin}$ are $K_{\rm kin} \geqslant 2\sigma_{K_{\rm kin}}$, where $\sigma_{\Delta M} = 0.629$ mag and $\sigma_{K_{\rm kin}} = 3.2$ km s^{-1}. These standard deviations are calculated for the M+13 bona fide membership list with usable data (30 stars), i.e., omitting M+13's (17) provisional and rejected members.

Figure 2, like Figure 8 in M+13, illustrates the kinematic and magnitude offsets plotted against each other. The figure includes all stars from M+13 (i.e., M+13's bona fide, provisional, and rejected members) with Gaia parallaxes and $G - G_{RP}$ colors. Stars with $K_{\rm kin}$ or ΔM values that place them within both 2σ boundaries, within errors, are henceforth considered to be high-probability members of ϵCA. Stars outside these bounds were reconsidered for membership on a case by case basis. For instance, the two magnitude outliers beyond $1\sigma_K$, HD 104036 and HD 104237A, are both A stars in the bluest region of the CMD. This region is not well fit by the empirical isochrone so the large ΔM is not enough to disqualify their membership. Additional cases, including stars whose DR2 parallaxes render their ϵCA membership doubtful, are discussed in Sections 4.1.2 and 4.1.3.

Figure 3 presents Gaia CMDs for the full sample of M+13 stars initially considered ϵCA members, i.e., for the stars listed in Table 1 (left panel) and for the final membership list, which is presented and discussed in Section 4.1.5 (right panel). The empirical isochrone in both panels is that found for the original 30 star data set (i.e., is the same as the SLFR curve in Figure 1). In the following, we describe the reasoning behind retaining or rejecting the $>2\sigma$ outliers plotted in Figure 2.

4.1.2. Candidates Rejected on the Basis of Kinematics, Photometry, and/or Parallaxes

We corroborate the rejected status of all of the eleven ϵCA members rejected by M+13. Five of the M+13 rejects clearly maintain their nonmember status on the basis of the large Gaia-based kinematic and magnitude offsets determined here (Table 2). One rejected M+13 member with offsets $<2\sigma$, 2MASS J12074597–7816064, is unlikely to be a member given its position in the Gaia CMD (Figure 1). This star falls below our empirical isochrone, despite being a suspected spectroscopic binary (M+13). Its kinematic offset is also at the edge of acceptability ($K_{\rm kin} = 3.03$ km s^{-1}). We hence exclude 2MASS J12074597–7816064 from our final ϵCA membership list. Another five M+13 rejected stars now convincingly lose membership status based on Gaia parallaxes (2MASS J11334926–7618399, RX J1243.1–7458, RX J1150.4–7704, TYC 9238-612-1, and TYC 9420-676-1). VW Cha, which was previously rejected on the basis of a pre-Gaia distance estimate, was not reconsidered in this work because no Gaia parallax was reported in DR2.

Table 2
Membership Quality Flags

Name	K_{kin}	$\sigma_{K_{kin}}$	ΔM	$\sigma_{\Delta M}$	Status	Notes
HD 8279	4.35	0.21	1.8911	0.0066	R	Previously rejected (Section 4.1.2)
CP-68 1388	2.0	1.0	−0.1975	0.0097	M	
2MASS J11183572−7935548A	4.7	1.6	−1.200	0.033	M	
RX J1123.2−7924	15.8	2.9	0.9509	0.0065	R	Previously rejected (Section 4.1.2)
HIP 55746	7.1	1.2	1.383	0.027	R	Previously rejected (Section 4.1.2)
RX J1137.4−7648	4.6	5.0	1.8790	0.0046	R	Previously rejected (Section 4.1.2)
2MASS J11404967−7459394	4.2	1.0	0.025	0.016	M	
2MASS J11411722−7315369	⋯	⋯	1.093	0.012	P	
2MASS J11432669−7804454	17.9	4.1	−0.83	0.24	R	Probable Cha Cloud (Section 4.1.2)
2MASS J11432968−7418377	⋯	⋯	0.8659	0.0090	P	
RX J1147.7−7842	1.81	0.90	−0.6586	0.0097	M	
RX J1149.8−7850	1.0	1.3	−0.0002	0.0097	M	
RX J1150.9−7411	2.7	1.3	−0.892	0.042	M	
2MASS J11550485−7919108	⋯	⋯	−0.059	0.015	M	
T Cha	3.0	1.3	−7.72	0.13	M	Anomalous CMD position (Section 4.1.3)
RX J1158.5−7754B	1.3	2.0	0.2454	0.0105	M	
RX J1158.5−7754A	3.6	1.8	−0.7542	0.0091	M	
HD 104036	1.87	0.51	3.5594	0.0092	M	
CXOU J115908.2−781232	1.22	0.25	0.774	0.015	M	
RX J1159.7−7601	1.3	3.7	0.3029	0.0073	M	
2MASS J12000269−7444068	⋯	⋯	0.799	0.012	P	
HD 104237A	0.69	0.42	2.21	0.016	M	
HD 104237D	⋯	⋯	−0.115	0.015	M	
HD 104237E	⋯	⋯	−1.027	0.036	M	
2MASS J12005517−7820296	3.4	1.3	−0.125	0.020	M	
HD 104467	1.6	1.0	0.010	0.038	M	
2MASS J12014343−7835472	5.93	0.65	4.168	0.045	M	Anomalous CMD position (Section 4.1.3)
USNO-B 120144.7−781926	0.83	1.11	0.064	0.022	M	
CXOU J120152.8−781840	2.5	1.1	0.33	0.0163	M	
RX J1202.1−7853	3.35	0.23	−0.279	0.013	M	
RX J1202.8−7718	0.77	0.61	0.365	0.010	M	
RX J1204.6−7731	3.6	2.0	−0.1695	0.0091	M	
HD 105234	⋯	⋯	3.1047	0.0083	P	
2MASS J12074597−7816064	1.5	1.9	1.029	0.014	R	Previously rejected (Section 4.1.2)
RX J1207.7−7953	1.01	0.70	0.3388	0.0087	M	
HIP 59243	⋯	⋯	3.2697	0.0075	P	
HD 105923	0.9	2.0	0.0231	0.0091	M	
RX J1216.8−7753	1.3	1.9	0.304	0.012	M	
RX J1219.7−7403	9.2	3.3	0.2485	0.0075	M	
RX J1220.4−7407	2.1	1.4	−1.09	0.24	R	Probable Cha Cloud (Section 4.1.2)
2MASS J12203396−7135188	⋯	⋯	−0.216	0.012	P	
2MASS J12203619−7353027	⋯	⋯	0.4854	0.0086	P	
2MASS J12210499−7116493	2.6	2.5	0.0482	0.0080	M	
2MASS J12220068−7001041	⋯	⋯	0.547	0.011	P	
2MASS J12222238−7137040	⋯	⋯	0.248	0.014	P	
2MASS J12224862−7410203	⋯	⋯	−0.822	0.021	P	
2MASS J12255824−7551116	⋯	⋯	⋯	0.784	0.015	P
2MASS J12324805−7654237	⋯	⋯	0.08	0.18	P	
2MASS J12332483−6848553	⋯	⋯	0.613	0.020	P	
2MASS J12351540−7043079	⋯	⋯	0.473	0.014	P	
RX J1239.4−7502	1.5	2.8	0.0672	0.0077	M	
2MASS J12421315−6943484	⋯	⋯	0.235	0.019	P	
RX J1243.1−7458	11.1	7.0	0.27	0.11	R	Previously rejected (Section 4.1.2)
2MASS J12425584−7034207	⋯	⋯	0.270	0.018	P	
2MASS J12473611−7031135	⋯	⋯	0.5594	0.0073	P	
CD-69 1055	2.5	1.9	0.1176	0.0087	M	
MP Mus	2.32	0.21	−0.2265	0.0097	M	

Note. Key for status column: M = member; P = provisional member; R = rejected.

Two stars previously considered bona fide ϵCA members by M+13, 2MASS J11432669−7804454 and RX J1220.4−7407, have CMD positions consistent with young ages and are marginally consistent with ϵCA membership (in terms of ΔM) given our SLFR analysis, although both were flagged as photometric binaries due to their elevation above the single-star locus. Kinematically, RX J1220.4−7407 lies within the distribution of ϵCA members ($K_{kin} = 2.11$ km s^{-1}), while 2MASS J11432669−7804454 has a
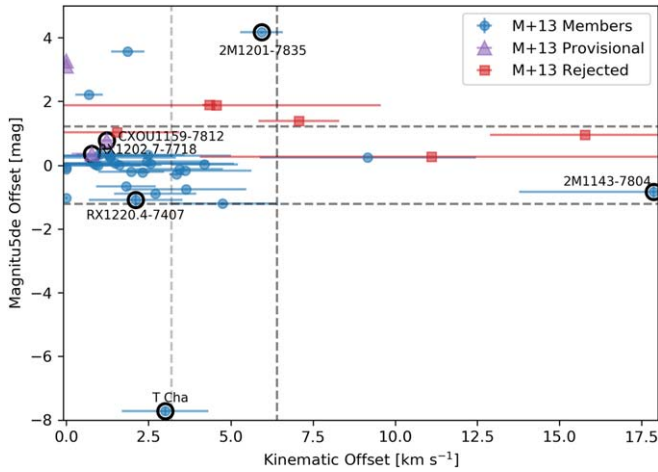
Figure 2. Comparison of the offsets in CMD (G vs. $G - R_p$) space and kinematic (UVW) space used to assess ϵCA membership (Section 4.1). Blue circles, purple triangles, and red squares represent the M+13 ϵCA study's bona fide members, provisional members, and rejected stars, respectively. The horizontal dashed lines correspond to $2\sigma_{\Delta M} = 1.25$ mag; the vertical dashed lines correspond to $\sigma_{K_{\rm kin}}$ (3.2 km s^{-1}) and $2\sigma_{K_{\rm kin}}$. Points appearing at 0.0 on the x-axis are stars lacking radial velocity measurements, for which kinematic offsets cannot be determined. Four outliers discussed in the text are labeled: RX J1220.4–7407 and 2MASS J11432669–7804454 in Section 4.1.2, T Cha and 2MASS J12014343–7835472 in Section 4.1.3, and RX J1202.8–7718 and CXOU J1159082–781232 in Section 4.1.4.

large kinematic offset (17.9 km s^{-1}). However, these stars have Gaia parallaxes of 5.54 and 6.71 mas, respectively, a factor of 1.5–2 smaller than the mean for ϵCA (9.81 mas). Notably, both stars have high RUWE and `astrometric_excess_noise` values, suggesting that their parallax solutions may not be reliable. If their parallaxes are in fact accurate, their relatively large distances would indicate they are younger, background T Tauri stars associated with the Cha star-forming region (see, e.g., Kastner et al. 2012). Their positions above the single-star locus would be consistent with their belonging to this (generally younger) Cha cloud population. Given these uncertainties, we do not include these two stars in our final roster of bona fide ϵCA members, although their status is worth revisiting in future Gaia data releases.

Of the six provisional members identified by M+13, two can be rejected outright based on their Gaia parallaxes: TYC 9414-191-1 ($\pi = 1.56$ mas) and CM Cha ($\pi = 5.15$ mas). TYC 9414-191-1 is likely a background star with proper motions similar to those of ϵCA members, and CM Cha (like 2MASS J11432669–7804454 and RX J1220.4–7407) appears to belong to the more distant Cha cloud T Tauri star population. The other four M+13 provisional members are discussed in Section 4.1.4.

4.1.3. Outliers Retained as Likely Members

T Cha: T Cha was previously established as a kinematic member of ϵCA (Torres et al. 2008). The kinematic analysis of T Cha is more complicated than other ϵCA members, however, due to its variable RV; measurements range from $\sim$6 to $\sim$30 km s^{-1} (Schisano et al. 2009). We adopt the RV measured by Guenther et al. (2007), 14.0 ± 1.3, which is near the median of the values reported by Schisano et al. (2009); with this RV, the UVW of T Cha (presented in Section 4.1.5) yield a $K_{\rm kin}$ of 3.0 ± 1.3 km s^{-1}, well within the 2σ region. Adopting a larger value for its RV (e.g., the Gaia DR2 RV, 25.52 ± 4.24) would make T Cha a kinematic outlier. However, its XYZ (52.7,

$-90.1, -31.4$ pc) positions T Cha near the median of ϵCA. We conclude that the Gaia DR2 astrometric data for T Cha support its membership in ϵCA, although the variable nature of its RV still remains to be characterized (see discussion in Schisano et al. 2009).

The Gaia DR2 photometric data for T Cha (Figure 1) show it to be far redder and fainter than expected for an ϵCA star of its spectral type and mass (G8 and 1.3 $M_\odot$, respectively; Schisano et al. 2009). In DR2, T Cha was flagged as having a suspect `phot_bp_rp_excess_factor` factor (i.e., $E = 2.2$), indicative of poor-quality photometry. This is perhaps due to the star's notable variable behavior: T Cha is known to exhibit variable extinction in the optical regime, as a consequence of its highly inclined, dusty disk ($i = 73°$; Hendler et al. 2018). Schisano et al. (2009) found that T Cha shows a visual extinction (corrected for ISM extinction) of $\sim$0.5 mag on average, but with large excursions, sometimes reaching a maximum of $\sim$3 mag. Variable extinction in young stars with disks, such as that displayed by T Cha, has been hypothesized to result from a nested inner/outer disk structure wherein a warped inner disk causes quasi-periodic occultations of the photosphere (Alencar et al. 2010). Modeling of the disk around T Cha shows that instead, its variability could be caused by an asymmetric, puffed-up inner disk rim (Olofsson et al. 2013).

Based on its position in the Gaia CMD (Figure 3, right) and assuming a spectral type of G8 (Schisano et al. 2009)—which suggests an absolute G magnitude of 3.3, given the SLFR-derived empirical isochrone (Figure 1)—and applying a standard ISM reddening law (Cardelli et al. 1989), we infer an A_V of 6.0 mag at the time of Gaia observations. This A_V is a factor of $\sim$10 larger than the typical A_V reported by Schisano et al. (2009)—a surprising result, given that (as of DR2) Gaia data included nine viable visibility periods. Alternatively, if we were to accept the $G - G_{RP}$ of T Cha at face value, then the star displays a color excess $E(G - G_{RP}) = 1.11$, which would imply $A_V \sim 3.5$ assuming T Cha's obscuration follows the same (Cardelli et al. 1989) standard reddening law. This is still a factor of $\sim$5 larger than typical for T Cha, and is furthermore discrepant with A_V as determined from its spectral-type-based absolute magnitude. Thus, while T Cha's anomalous position in the ϵCA CMD is likely due in part to obscuration by its disk, and suggests the disk dust exhibits non-ISM-like reddening, we caution that its position (low and red) in the CMD may also be a consequence of suspect Gaia photometry.

2MASS J12014343–7835472: This early-M star (M2.25; Luhman 2004), also known as ϵCA 11, is notably under-luminous for a star in this spectral type regime ($\Delta M \sim 4$ mag; Figure 1). Previous studies of ϵCA have proposed that 2MASS J12014343–7835472 is orbited by a nearly edge-on disk (Luhman 2004), such that the cold, outer parts of the disk flare to block the stellar photospheric emission, which is then only detected in the form of scattering off the inner disk (Fang et al. 2013). The star also appears to be actively accreting disk material, given its large Hα equivalent width (Luhman 2004).

Although 2MASS J12014343–7835472 has a large $K_{\rm kin}$ value (5.7 km s^{-1}), this is mainly due to its low measured RV (11.44 $\pm$ 2.53 km s^{-1}); its Gaia DR2 proper motions are generally consistent with those of other ϵCA members. Furthermore, its lithium absorption-line (λ6708) equivalent width is consistent with the young age of the ϵCA (M+13). Its membership in ϵCA is hence supported by the available data, provided its photospheric emission is indeed strongly attenuated by a nearly edge-on disk.
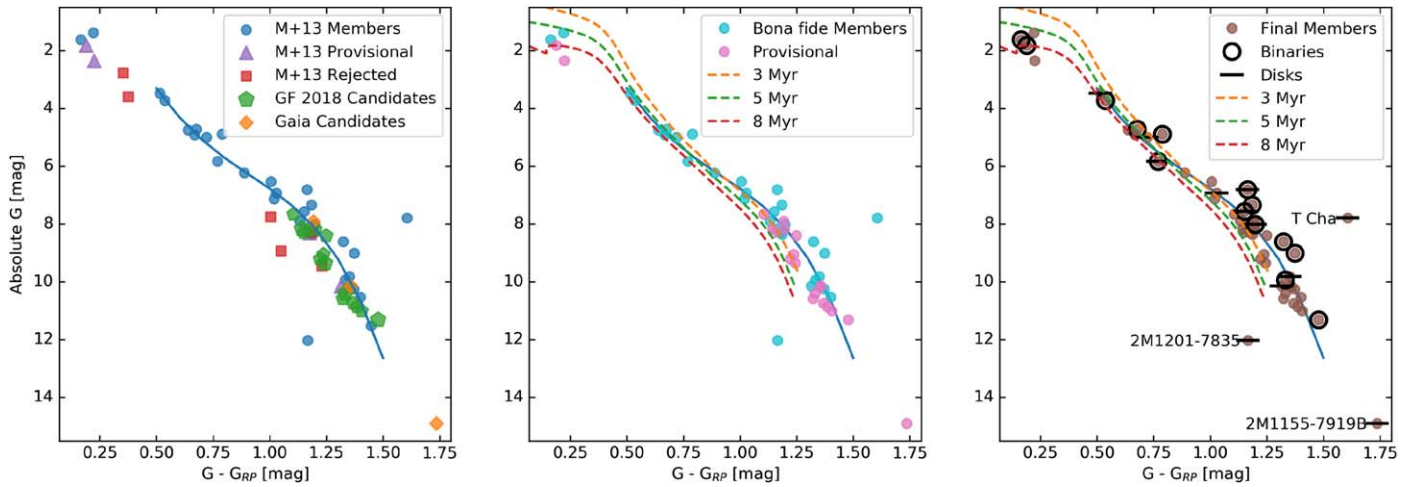
Figure 3. Gaia DR2 CMDs for the initial sample of stars considered for ϵCA membership (Table 1; left panel) and for our final member lists, both bona fide and provisional members (Tables 3, 4); center and right panels). The empirical isochrone obtained from SLFR analysis of the original 30 bona fide members from M+13 (Figure 1) is overlaid in all three panels (blue curves). In the left panel, the blue circles, purple triangles, and red squares indicate M+13 membership candidacy (as in Figure 2); new candidate ϵCA members identified via our wide-separation companion search (Section 4.2.2) are represented by orange diamonds; and candidates originating from GF18 are represented with green pentagons. In the center panel, our final confirmed ϵCA members (Table 3 are indicated with brown circles and our provisional ϵCA members (Table 4) are indicated with pink circles. This panel and the right panel also include theoretical isochrones (dashed curves) from Tognelli et al. (2018) for ages of 3.0 Myr (orange), 5.0 Myr (green), and 8.0 Myr (red). In the right panel, both provisional and confirmed ϵCA members (Tables 3 and 4) are represented with brown circles; black dashes indicates stars with disks and black open circles indicate Gaia unresolved binaries and photometric binary candidates. Three stars of particular interest, discussed in the text, are labeled: T Cha (Section 4.1.3), 2MASS J12014343–7835472 (Section 4.1.3), and 2MASS J11550336–7919147 (Section 4.2.2).

Unlike T Cha, the $G - G_{R_P}$ color of 2MASS J12014343–7835472 appears consistent with its spectral type (Figure 1), suggesting that the occulting disk dust has a significant component of large grains even as the Gaia photometry is dominated by starlight scattered off the disk surface.

4.1.4. Other ϵCA Candidates

Provisional M+13 candidates: Two stars designated as provisional ϵCA members in the M+13 ϵCA study, RX J1202.8–7718 and CXOU J115908.2–781232, are upgraded here to bona fide members. RX J1202.8–7718 was identified as a kinematic member in M+13 but its status was uncertain, with the possibility remaining that it could belong to the Lower Centaurus Crux (LCC) subgroup of the Scorpius-Centaurus OB association. In our analysis, RX J1202.8–7718 has both low K_{kin} (0.31 km s^{-1}) and ΔM (0.39 mag), suggesting that it is unlikely to be an interloper from the LCC. Likewise, on the basis of its pre-Gaia proper motion and distance, M+13 suspected that CXOU J115908.2–781232 may be associated with the Cha I cloud. However, Gaia DR2 places the star at ∼105 pc, consistent with ϵCA and much nearer to Earth than Cha I. Given its low K_{kin} (0.31 km s^{-1}) and ΔM (0.82 mag), we include CXOU J115908.2–781232 among our bona fide ϵCA member list.

Two other M+13 provisional members, HD 105234 and HIP 59243, lack the requisite RVs to determine their *UVW* and, hence, kinematic offsets, and are thus also classed as provisional members in our final membership list. Therefore, of the six provisional members presented by M+13, two are rejected, two are upgraded to bona fide, and two maintain their provisional status.

Gagné & Faherty (2018) candidates: On the basis of a statistical analysis of Gaia DR2 data (utilizing BANYAN; Gagné et al. 2018c), GF18 identified a total of 15 stars that are candidate members of ϵCA. These stars were designated as high-probability members (five stars), possible members (five), and low-probability members (five), based on BANYAN probabilities of membership in ϵCA as well as in other young moving groups. Their *XZ* distribution (Figure 4, left panel) makes apparent that the GF18 high-probability members are found within the spatial locus of stars we designate as bona fide ϵCA members—albeit outside the core ϵCA group (centered at $X \sim 49$ pc, $Z \sim -28$ pc), because the GF18 study excluded stars with distances >100 pc, whereas the lower-probability members are found at the upper *XZ* periphery of the group.

In contrast, there is no such clear distinction between the CMD positions of the three categories of GF18 candidates. All 15 stars lie along the single-star CMD locus of ϵCA determined via our SLFR analysis, although most (13 of 15) lie below the empirical isochrone, by up to a magnitude (Figure 4, right panel). While this might cast doubt on their ϵCA membership, we caution that most of the GF18 stars lie in a region of CMD space that is poorly sampled by kinematically verified ϵCA members. Hence, the final membership status of all 15 stars is not easily assessed and must await measurements of, e.g., RVs and Li absorption-line strengths.

To assign spectral types to the provisional ϵCA members gleaned from the GF18 study, as well as other provisional members (Section 4.1.5), we have determined an empirical relationship between spectral subtype and Gaia color for bona fide K- and M-type ϵCA members. For this purpose, we selected those K and M stars from our final membership list (Section 4.1.5) for which spectral types were determined from optical spectroscopy and for which $E(B - V) \leqslant 0.05$, based on data presented in M+13. The resulting empirical relationship is illustrated in Figure 5. The best-fit second-order polynomial shown in the Figure is given by

$$\mathrm{Sp}(c) = -12.78c^2 + 42.54c - 29.26, \qquad (3)$$

where Sp is the spectral index of the star, defined such that $(...-1, 0, +1, ...) = (...K7, M0, M1, ...)$, and c is the $G - G_{RP}$ color. Figure 5 demonstrates that Equation (3) provides an
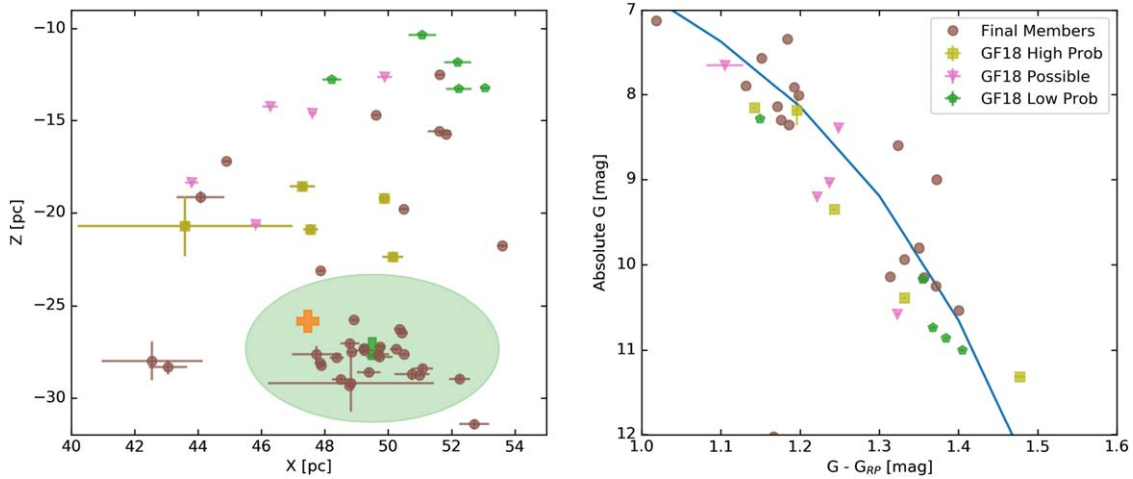
Figure 4. Individual components of heliocentric positions (*XZ*) and the Gaia CMD for both the final membership list of ϵCA (Table 3; brown circles) and GF18 ϵCA candidates. Yellow squares, pink triangles, and green pentagons indicate GF18's high-probability, possible, and low-probability members, respectively. In the left panel, the heliocentric median and mean positions for ϵCA members (Table 7) are indicated as green and orange plus signs, respectively. The green shaded region represents the area within the inferred tidal radius (∼4 pc; Section 5.2) as centered on the median position.

accuracy of roughly a subtype for K and M stars in the ϵCA. The spectral types determined from this empirical color–subtype relationship for the provisional members from GF18 are, in most cases, 0.5–2.0 subtype later than those reported by GF18. Our determinations are likely to be more reliable, however, given that they are based on the Gaia colors of bona fide ϵCA members of known spectral type, and the color–subtype relationship is known to be age-dependent (e.g., Pecaut & Mamajek 2013).

4.1.5. Final ϵCA Membership; Provisional Members

Our final ϵCA membership list, including spectral types, distances, Gaia photometry, and 2MASS photometry (Skrutskie et al. 2006), is presented in Table 3. Most ϵCA candidates without RVs are here designated as provisional members—the exceptions being three systems lacking RVs that were classified as bona fide members by M+13, for which we find Gaia DR2-based *XYZ* and CMD positions that are consistent with membership. The provisional members are presented in Table 4. The latter list includes three new members revealed via a search for wide-separation companions (Table 5; see Section 4.2.2).

For each star in Tables 3 and 4, we also indicate stellar multiplicity and the presence/absence of evidence of a circumstellar disk. Multiplicity is further subdivided into photometric binaries (P), visual binaries from Briceño & Tokovinin (2017; V), suspected spectroscopic binaries from M+13 (S), and candidate wide-separation companion systems (C). Binarity and multiplicity within the final membership list are further discussed in Section 4.2.

Table 6 lists the heliocentric space positions (*XYZ*) and velocities (*UVW*) of the final ϵCA membership. The medians and (uncertainty-weighted) means of these spatial and kinematic coordinates, as calculated from the positions and velocities of bona fide members in Table 3, are tabulated in Table 7.

Figure 6 illustrates the individual and mean positions and velocities. Based on our final membership, the mean distance to the ϵCA is 100.99 pc, with a standard deviation $\sigma = 4.62$ pc. The structure and spectral type distribution of the association are discussed in Section 5.2.
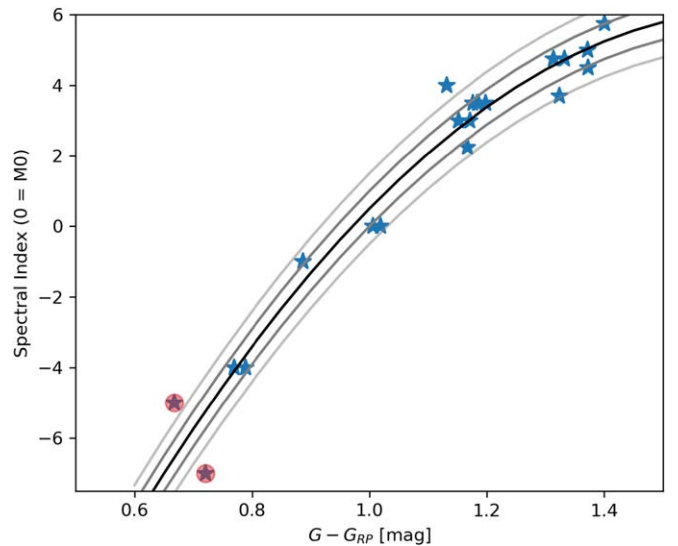

Figure 5. Spectral index vs. Gaia $G - G_{RP}$ color for all M+13 members with $E(B - V) \leqslant 0.05$. Spectral index is here defined such that $(...-1, 0, +1, ...) = (...K7, M0, M1, ...)$. Most stars have inferred $E(B - V) = 0.0$; two stars with $E(B - V) = 0.05$ are marked with red circles. The black curve represents the best-fit second-order polynomial, and the dark and light gray curves represent deviations of 0.5 and 1.0 subtype, respectively.

4.2. Multiplicity

4.2.1. Photometric Binaries

On the basis of our SLFR analysis, we identify five photometric binary candidates, i.e., stars that lie above the single-star locus at positions consistent with their being double or perhaps triple systems: RX J1150.9−7411, RX J1158.5−775A, HD 104237E, RX J1147.7−7842, and 2MASS J11183572−7935548. These stars have ΔM values of −1.211, −0.670, −0.903, −0.767, and −1.038, respectively. Two of these systems, RX J1150.9−7411 and RX J1158.5−775A, have been resolved visually (separations 0″875 and 0″073, respectively; Köhler 2001; Briceño & Tokovinin 2017), but evidently, even the former is unresolved in Gaia DR2.

HD 104237E is already known to have a companion, HD 104237D (at separation 4″24; Briceño & Tokovinin 2017), and

Table 3
Final ε Cha Association Membership List[a]

Name	SpT	Distance (pc)[b]	G_{BP}	G	G_{RP}	J	H	K	Multiplicity[c]	Disk?[d]
CP-68 1388	K1	$115.66^{+0.39}_{-0.38}$	10.568	10.023	9.347	8.48	8.01	7.79	⋯	⋯
2MASS J11183572−7935548A	M4.5	$94.14^{+1.34}_{-1.30}$	15.513	13.869	12.50	10.50	9.89	9.62	P	⋯
2MASS J11183572−7935548B*	⋯	$93.04^{+3.61}_{-3.35}$	⋯	16.189	⋯	⋯	⋯	⋯	⋯	⋯
2MASS J11404967−7459394	M5.5	$95.68^{+0.64}_{-0.64}$	18.833	16.429	14.983	12.68	12.15	11.77	⋯	⋯
RX J1147.7−7842	M3.5	$100.52^{+0.39}_{-0.39}$	13.814	12.352	11.168	9.52	8.86	8.59	P	⋯
RX J1149.8−7850	M0	$100.28^{+0.25}_{-0.25}$	13.0419	11.932	10.904	9.45	8.72	8.49	⋯	Y
RX 1150.9−7411	M3.7	$93.61^{+1.62}_{-1.56}$	14.852	13.457	12.133	10.38	9.78	9.48	VP	⋯
2MASS J11550485−7919108	M3	$100.60^{+0.60}_{-0.59}$	16.826	14.818	13.468	11.22	10.47	10.08	C	Y
T Cha	G8	$108.98^{+0.99}_{-0.97}$	13.682	12.974	11.368	8.96	7.86	6.95	⋯	Y
RX J1158.5−7754B	M3	$102.92^{+0.37}_{-0.37}$	14.629	13.202	12.031	10.34	9.72	9.44	⋯	⋯
RX J1158.5−7754A	K4	$104.47^{+0.39}_{-0.38}$	10.688	9.980	9.191	8.22	7.56	7.40	VP	⋯
HD 104036	A7	$103.95^{+0.42}_{-0.41}$	6.806	6.693	6.528	6.29	6.22	6.11	V	⋯
CXOU J115908.2−781232*	M4.75	$105.50^{+0.69}_{-0.68}$	17.118	15.256	13.942	12.01	11.45	11.17	⋯	Y
ε Cha AaAbB	B9	111H	4.862	4.782	4.931	5.02	5.04	4.98	V	⋯
RX J1159.7−7601	K4	$99.21^{+0.23}_{-0.23}$	11.491	10.809	10.040	9.14	8.47	8.30	⋯	⋯
HD 104237C	M/L	⋯	⋯	⋯	⋯	⋯	⋯	⋯	⋯	⋯
HD 104237B	K/M	⋯	⋯	⋯	⋯	⋯	⋯	⋯	⋯	⋯
HD 104237A	A7.75	$107.76^{+0.68}_{-0.67}$	6.710	6.543	6.321	5.81	5.25	4.59	⋯	Y
HD 104237D	M3.5	$100.61^{+0.62}_{-0.62}$	14.440	13.021	11.823	9.62	8.74	8.12	⋯	?
HD 104237E	K5.5	$101.52^{+0.35}_{-0.34}$	12.653	11.838	10.675	⩾9.10	⩾8.25	7.49	P	Y
2MASS J12005517−7820296	M5.75	$102.39^{+0.87}_{-0.85}$	17.865	15.583	14.182	11.96	11.40	11.01	S	Y
HD 104467	G3	$98.11^{+1.62}_{-1.56}$	8.796	8.428	7.914	7.26	6.97	6.85	C	⋯
2MASS J12014343−7835472	M2.25	$104.334^{+1.16}_{-1.13}$	18.205	17.115	15.949	14.36	13.38	12.81	⋯	Y
USNO-B 120144.7−781926	M5	$101.29^{+0.65}_{-0.64}$	17.248	15.276	13.904	11.68	11.12	10.78	⋯	Y
CXOU J120152.8−781840	M4.75	$102.16^{+0.71}_{-0.70}$	16.939	14.982	13.650	11.63	11.04	10.77	⋯	⋯
RX J1202.1−7853	M0	$99.36^{+0.46}_{-0.45}$	12.547	11.510	10.504	9.215	8.46	8.31	V	⋯
RX J1202.8−7718*	M3.5	$103.52^{+0.37}_{-0.37}$	14.795	13.375	12.199	10.51	9.83	9.59	⋯	⋯
RX J1204.6−7731	M3	$100.24^{+0.34}_{-0.33}$	13.94	12.571	11.420	9.77	9.13	8.88	⋯	⋯
RX J1207.7−7953	M3.5	$99.30^{+0.30}_{-0.30}$	14.793	13.340	12.154	10.43	9.76	9.57	⋯	⋯
HD 105923	G8	$105.78^{+0.41}_{-0.40}$	9.245	8.837	8.300	7.67	7.31	7.18	VC	⋯
RX J1216.8−7753	M4	$101.27^{+0.40}_{-0.40}$	14.236	12.921	11.789	10.09	9.47	9.24	⋯	⋯
RX J1219.7−7403	M0	$100.82^{+0.27}_{-0.27}$	13.201	12.140	11.121	9.75	9.05	8.86	⋯	⋯
2MASS J12210499−7116493	K7	$98.92^{+0.24}_{-0.23}$	12.044	11.203	10.316	9.09	8.42	8.24	⋯	⋯
RX J1239.4−7502	K3	$103.10^{+0.29}_{-0.28}$	10.531	9.975	9.307	8.43	7.95	7.78	⋯	⋯
CD-69 1055	K0	$94.32^{+0.26}_{-0.26}$	10.132	9.606	8.967	8.18	7.70	7.55	⋯	⋯
MP Mus	K1	$98.34^{+0.30}_{-0.30}$	10.547	9.952	9.231	8.28	7.64	7.29	⋯	Y

Notes.
[a] * = previously not considered a bona fide member (M+13).
[b] Distances have been calculated using the inverse parallax method with zero-point corrections (Lindegren et al. 2018).
[c] S = suspected spectroscopic binary (M+13); V = resolved binary (Briceño & Tokovinin 2017); P = possible photometric binary (this work); C = potential wide-separation companion (this work).
[d] IR excess and/or other evidence indicative of presence of circumstellar disk (M+13 and references therein).

would be a hierarchical triple system if HD 104237E is confirmed as a binary (see Section 4.2.3). The DR2-based binary candidacy of RX J1147.7−7842 is also novel. Both systems warrant spectroscopic follow-up to search for RV variability, since close binaries can have suspect Gaia DR2 astrometry (e.g., Kastner 2018). We note that Briceño & Tokovinin (2017) failed to detect companions at separations as small as ∼0″1 (∼10 au) for these two stars.

Briceño & Tokovinin (2017) found that the 2MASS J11183572−7935548 system (henceforth J1118AB) is a 0″92 separation binary consisting of an M4.5 primary and a lower-luminosity companion that may be related to the transition-disk nature of the object. The Gaia DR2 data confirm the angular separation (0″9) and establish that this corresponds to a projected physical separation of 85 au. The parallaxes for J1118AB agree, within the errors, confirming that they constitute a physical pair. Unfortunately, the only Gaia photometry for J1118B is in the G band, so we could not ascertain the CMD location of this companion. J1118A was flagged as a spectroscopic binary in M+13 and, via our SLFR method, we find it is also a candidate photometric binary. In light of the presence of the faint visual companion 2MASS 1118B (Briceño & Tokovinin 2017), it appears that 2MASS 1118AB is a possible hierarchical triple system.

4.2.2. Wide-separation Binaries

We searched for potential wide-separation companions to all εCA members retained after applying the criteria described in Section 4.1. Specifically, we searched the Gaia DR2 catalog for

Table 4
Provisional ϵ Cha Association Membership List

Name	SpT[a]	Distance (pc)[b]	G_{BP}	G	G_{RP}	J	H	K	Multiplicity[c]	Disk?[d]
2MASS J11411722−7315369	M4.5	$95.51^{+0.47}_{-0.47}$	17.382	15.478	14.155	12.16	11.56	11.31	⋯	⋯
2MASS J11432968−7418377	M3.5	$98.84^{+0.38}_{-0.38}$	15.742	14.176	12.955	11.25	10.60	10.37	⋯	⋯
2MASS J11550336−7919147	M6	$101.26^{+5.70}_{-5.12}$	20.476	19.925	18.189	15.85	15.03	⩾ 12.64	⋯	Y
2MASS J12000269−7444068	M4	$98.80^{-0.48}_{+0.48}$	15.959	14.324	13.081	11.37	10.67	10.42	⋯	⋯
2MASS J12011981−7859057	M5	$101.55^{+0.78}_{-0.77}$	17.251	15.179	13.823	11.75	11.20	10.89	⋯	⋯
HD 105234	A9‡	$103.96^{+0.38}_{-0.37}$	7.570	7.419	7.195	6.87	6.76	6.68	V	Y
HIP 59243	A6‡	$99.27^{+0.32}_{-0.32}$	6.934	6.794	6.605	6.35	6.23	6.17	V	⋯
2MASS J12115619−7108143	M3	$105.28^{+0.76}_{-0.75}$	14.530	13.021	11.828	10.09	9.51	9.24	⋯	⋯
2MASS J12203396−7135188	M4	$92.36^{+0.49}_{-0.48}$	14.880	13.219	11.971	10.14	9.57	9.27	⋯	⋯
2MASS J12203619−7353027	M2.5	$99.40^{+0.35}_{-0.34}$	14.485	13.141	11.998	10.41	9.71	9.48	⋯	⋯
2MASS J12220068−7001041	M4	$99.39^{+0.47}_{-0.47}$	15.402	14.024	12.787	⩾ 10.40	⩾ 10.00	⩾ 9.90	⋯	⋯
2MASS J12222238−7137040	M2	$94.61^{+0.25}_{-0.24}$	13.769	12.530	11.425	9.90	9.27	8.99	⋯	⋯
2MASS J12224862−7410203	M5.5	$93.82^{+0.79}_{-0.78}$	18.688	16.175	14.698	12.26	11.69	11.29	P	⋯
2MASS J12255824−7551116	M4.5	$98.98^{+0.64}_{-0.63}$	17.324	15.366	14.034	12.02	11.49	11.19	⋯	⋯
2MASS J12324805−7654237	M3	$85.17^{+7.14}_{-6.11}$	14.310	12.835	11.639	9.88	9.26	8.96	⋯	⋯
2MASS J12332483−6848553	M5	$98.86^{+0.85}_{-0.83}$	17.829	15.712	14.344	12.28	11.68	11.37	⋯	⋯
2MASS J12351540−7043079	M5	$92.94^{+0.57}_{-0.56}$	17.853	15.701	14.317	12.18	11.66	11.33	⋯	⋯
2MASS J12421315−6943484	M5	$98.85^{+0.82}_{-0.80}$	17.167	15.144	13.789	11.76	11.15	10.87	⋯	⋯
2MASS J12425584−7034207	M5	$98.86^{+0.77}_{-0.75}$	18.261	15.975	14.570	12.32	11.79	11.46	⋯	⋯
2MASS J12473611−7031135	M3	$99.35^{+0.31}_{-0.30}$	14.628	13.269	12.119	10.50	9.86	9.71	⋯	⋯

Notes.
[a] Spectral types determined.
[b] Distances have been calculated using the inverse parallax method with zero-point corrections (Lindegren et al. 2018).
[c] S = suspected spectroscopic binary (M+13); V = resolved binary (Briceño & Tokovinin 2017); P = possible photometric binary (this work).
[d] IR excess and/or other evidence indicative of presence of circumstellar disk (M+13 and references therein).

Table 5
New Wide-separation Companions to ϵCA Members[a]

Name	SpT	R.A. (deg)	Decl. (deg)	π (mas)	G (mag)	$G - G_{RP}$ (mag)	PMRA (mas yr^{-1})	PMDec (mas yr^{-1})
2MASS J11550485−7919108	M3	178.7692	−79.3198	9.886 ± 0.058	14.818	1.35	−41.18 ± 0.13	−4.34 ± 0.09
2MASS J11550336−7919147	M6	178.7628	−79.3208	9.82 ± 0.53	19.92	1.74	−39.74 ± 1.22	−4.66 ± 0.68
HD 104467	G3	180.4120	−78.9881	10.14 ± 0.17	8.428	0.515	−41.11 ± 0.26	−5.41 ± 0.26
2MASS J12011981−7859057	M5	180.3316	−78.9849	9.794 ± 0.075	15.179	1.3562	−41.99 ± 0.12	−5.35 ± 0.10
HD 105923	G8	182.9084	−71.1767	9.400 ± 0.036	8.837	0.537	−38.720 ± 0.060	−7.42 ± 0.05
2MASS J12115619−7108143	M3	182.9836	−71.1374	9.44 ± 0.68	13.021	1.1928	−38.64 ± 0.11	−8.11 ± 0.09

Note.
[a] Candidate wide-separation comoving systems are listed as pairs, with the previously identified ϵCA member listed first and its candidate wide-separation companion listed second.

equidistant, comoving stars by querying the catalog for all Gaia sources within a 500″ radius of the position of each of these ϵCA members and then reordering the resulting source list by parallax. This search radius corresponds to ∼50 kau, or ∼0.25 pc, at the mean distance to ϵCA. While a search of ϵCA member fields within this radius typically returns ∼2000 stars, once ordered by parallax, potential (equidistant) companions to the star originally queried rise to the top of the list and are hence conspicuous. All stars so identified have parallaxes and proper motions within a few percent of the star searched and so were accepted as wide-separation companion candidates.

Applying this method, we have identified three new candidate members of ϵCA. Gaia DR2 data for these candidates are listed in Table 5. The faintest and reddest of these three, 2MASS J11550336−7919147, is described below. The other two

comoving companion candidates, 2MASS J12011981−7859057 and 2MASS J12115619−7108143, are mid-M stars that fall along the empirical single-star isochrone, with $\Delta M \leqslant 2\sigma_{\Delta M}$. These two candidate comoving companions have projected physical separations from their primaries of 5.7 kau and 17.7 kau, respectively. We estimated their spectral types (M5 and M3, respectively) from the empirical relationship between Gaia $G - G_{RP}$ color and spectral type for ϵCA members described in Section 4.1.4. Neither star displays evidence of a dusty disk in the form of an IR excess, i.e., both have 2MASS/WISE colors consistent with those of "diskless" young-M stars of similar spectral type (Pecaut & Mamajek 2013).

This comoving companion search also recovered multiple stars already considered ϵCA members as components of possible wide binary systems. The RX J1158.5−7754 system was matched with

Table 6
Bona Fide εCA Members: Heliocentric Positions and Velocities

Name	X	σ	Y	σ	Z	σ	U	σ	V	σ	W	σ
				(pc)						(km s^{-1})		
CP−68 1388	44.89	0.15	−105.20	0.35	−17.209	0.057	−10.86	0.39	−20.69	0.91	−8.72	0.15
2MASS J11183572−7935548A	43.049	0.605	−78.8	1.1	−28.32	0.40	−7.80	0.77	−23.6	1.3	−10.37	0.50
2MASS J11183572−7935548B	42.5	1.6	−77.9	2.9	−28.0	1.0	…	…	…	…	…	…
RX J1147.7−7842	47.86	0.19	−83.82	0.33	−28.09	0.11	−9.54	0.44	−20.99	0.75	−11.23	0.25
RX J1149.8−7850	47.89	0.12	−83.46	0.21	−28.230	0.071	−10.87	0.62	−18.8	1.1	−10.39	0.37
RX 1150.9−7411	44.08	0.75	−80.3	1.4	−19.16	0.33	−7.88	0.64	−19.3	1.0	−10.57	0.29
2MASS J11550485−7919108	48.51	0.29	−83.23	0.49	−28.98	0.17	…	…	…	…	…	…
T Cha	52.712	0.474	−90.06	0.81	−31.43	0.28	−11.98	0.65	−19.4	1.1	−13.03	0.38
RX J1158.5−7754B	49.75	0.18	−85.89	0.31	−27.220	0.098	−10.45	0.97	−18.5	1.7	−10.00	0.53
RX J1158.5−7754A	50.50	0.19	−87.18	0.32	−27.62	0.10	−10.06	0.88	−18.3	1.5	−13.71	0.48
HD 104036	50.25	0.20	−86.80	0.35	−27.34	0.11	−11.49	0.25	−18.26	0.41	−11.07	0.14
CXOU J115908.2−781232	51.08	0.33	−87.83	0.57	−28.40	0.19	−9.45	0.16	−20.27	0.18	−10.398	0.076
RX J1159.7−7601	47.87	0.11	−83.77	0.19	−23.116	0.053	−10.4	1.8	−18.7	3.1	−9.65	0.86
HD 104237A	52.25	0.33	−89.68	0.56	−28.96	0.18	−10.85	0.23	−19.15	0.33	−10.60	0.12
HD 104237D	48.79	0.30	−83.73	0.52	−27.04	0.17	…	…	…	…	…	…
HD 104237E	49.23	0.17	−84.49	0.29	−27.290	0.093	…	…	…	…	…	…
2MASS J12005517−7820296	49.72	0.42	−85.09	0.71	−27.76	0.23	−11.92	0.65	−16.9	1.1	−9.01	0.36
HD 104467	47.74	0.77	−81.1	1.3	−27.63	0.45	−10.39	0.55	−18.32	0.81	−9.65	0.30
2MASS J12014343−7835472	50.75	0.56	−86.52	0.95	−28.71	0.32	−8.02	0.36	−24.72	0.51	−12.37	0.19
USNO-B 120144.7−781926	49.26	0.32	−84.16	0.54	−27.42	0.18	−10.02	0.55	−20.34	0.92	−10.61	0.30
CXOU J120152.8−781840	49.69	0.34	−84.88	0.59	−27.62	0.19	−9.02	0.55	−21.44	0.92	−11.36	0.30
RX J1202.1−7853	48.37	0.22	−82.22	0.38	−27.80	0.13	−10.18	0.13	−23.05	0.17	−10.661	0.067
RX J1202.8−7718	50.37	0.18	−86.55	0.31	−26.265	0.094	−9.85	0.30	−19.89	0.50	−10.11	0.16
RX J1204.6−7731	48.92	0.17	−83.61	0.28	−25.761	0.087	−11.98	0.98	−16.67	1.67	−9.11	0.52
RX J1207.7−7953	48.77	0.15	−81.38	0.25	−29.325	0.089	−9.88	0.35	−20.29	0.58	−10.92	0.21
HD 105923	51.83	0.20	−90.86	0.35	−15.736	0.060	−9.64	0.52	−20.67	0.91	−8.76	0.16
RX J1216.8−7753	50.43	0.20	−83.74	0.33	−26.46	0.10	−9.7	1.0	−19.5	1.6	−10.39	0.52
RX J1219.7−7403	50.50	0.14	−84.98	0.23	−19.808	0.053	−9.71	0.95	−20.02	1.59	−9.40	0.37
2MASS J12210499−7116493	49.61	0.12	−84.31	0.20	−14.713	0.035	−10.5	1.3	−18.16	2.16	−8.38	0.38
RX J1239.4−7502	53.60	0.15	−85.33	0.24	−21.772	0.060	−9.3	1.5	−19.8	2.3	−9.66	0.59
CD−69 1055	51.63	0.14	−77.94	0.22	−12.501	0.034	−9.8	1.0	−18.7	1.6	−8.28	0.25
MP Mus	56.85	0.17	−79.36	0.24	−11.857	0.036	−9.13	0.13	−19.64	0.17	−8.566	0.043

Table 7
Mean and Median Heliocentric Positions and Velocities of εCA Members

	Mean[a]	Median	σ[b]
Distance (pc)	100.99	100.81	4.62
X (pc)	49.660	49.650	2.854
Y (pc)	−84.328	−84.232	5.185
Z (pc)	−18.905	−27.378	5.143
U (km s^{-1})	−9.847	−9.954	1.089
V (km s^{-1})	−20.667	−19.557	1.788
W (km s^{-1})	−9.682	−10.382	1.305

Notes.
[a] Weighted means and medians as calculated from values listed in Table 6.
[b] Standard deviation of the corresponding weighted mean.

HD 104036. Three stars, 2MASS J12005517−7820296, CXOU J120152.8−781840, and USNO-B 120144.7−781926, were identified as a three-component comoving system. We also identified CXOU J115908.2−781232, a provisional M+13 member, as another possible component of the HD 104237 multiple system (see Section 4.2.3).

2MASS J11550336−7919147: The third, newly identified wide-comoving companion, 2MASS J11550336−7919147 (henceforth 2MASS J1155−7919B), at an absolute G magnitude of ∼15 and G − G$_{RP}$ ∼ 1.75, is both the faintest and the reddest object thus far identified in εCA (Dickson-Vandervelde et al. 2020). As described in Dickson-Vandervelde et al. (2020), we find 2MASS J1155−7919B is comoving with 2MASS 11550485−7919108 (hereafter 2MASS J1155−7919A). The star 2MASS J1155−7919A was itself initially thought to be a wide-separation comoving companion to T Cha Kastner et al. (2012), before Gaia DR2 data established that T Cha and J1155−7919A are neither equidistant nor precisely comoving (Kastner 2018). The 2MASS J1155−7919AB pair has a projected separation of 5″.75, corresponding to a projected physical separation of 566 au. In Dickson-Vandervelde et al. (2020), we suggested that the position of 2MASS J1155−7919B at the extreme faint, red end of the single-star locus of the εCA CMD reflected its likely status as a substellar object, with a bolometric luminosity ($\log L_{bol}/L_\odot = -3.2$) that would imply its mass is a mere ∼10 M_{Jup}. This would make 2MASS J1155−7919B the lowest-mass εCA member presently known—even less massive than WISEA J120037.79−784508.3, a recently identified brown dwarf candidate and possible εCA member (Schutte et al. 2020)[5] However, a potential alternative model to explain the large absolute G magnitude and red color of 2MASS J1155−7919B is that the object is in fact a mid-M star—possibly a near-twin to host 2MASS J1155−7919A—that is obscured by a large column density of gray dust in a nearly edge-on disk. Under this interpretation, 2MASS J1155−7919B would be analogous to 2MASS J12014343−7835472 (=εCA 11; 4.1.3), but even

_____

[5] WISEA J120037.79−784508.3, which has an absolute G magnitude of 11.3, is not included in Table 4.
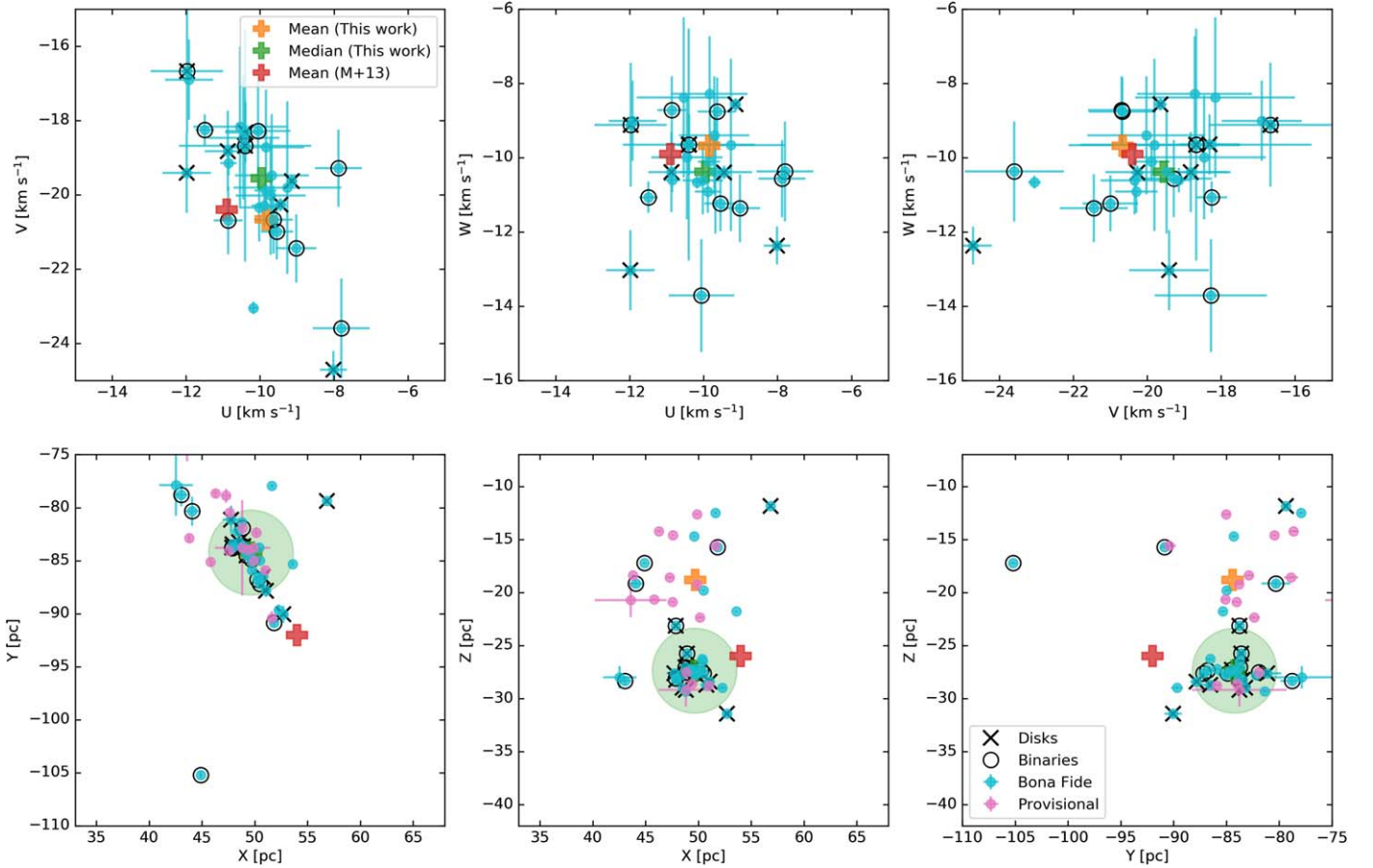
Figure 6. Individual components of heliocentric positions (*XYZ*) and velocities (*UVW*) plotted against one another for the final membership list (Table 3, cyan circles) and the provisional members (Tables 4, pink circles), with open black circles marking stars that are unresolved binaries and black Xs marking stars with disks. Table 3 stars lacking measured RVs (see Table 1) are omitted from the *UVW* plots. The mean and median values of *UVW* and *XYZ* are indicated by orange and green crosses, respectively, in each plot; the previously obtained mean values (from M+13) are represented by red crosses. The region within the calculated tidal radius (4 pc, Section 5.2) is indicated as a green circle in the *XYZ* plots, centered on the median. When no error bar can be seen, the error lies within the marker.

more highly obscured by its disk. Such an alternative explanation is motivated by the fact that 2MASS J1155 −7919B is consistently 5 mag dimmer than its host in *G*, *B_p*, *R_p*, *J*, and *H* (Table 5), and that its spectral type, as obtained from its color (via the relationship in Figure 5), is M6. In a forthcoming paper (D. A. Dickson-Vandervelde et al. 2020, in preparation), we further explore these two possible scenarios for the nature of 2MASS J1155−7919B.

4.2.3. HD 104237

HD 104237 is a proposed quintuplet system within ϵCA, consisting of a triple system dominated by the bright Herbig Ae/Be star HD 104237A and including the close binary HD 104237DE (Feigelson et al. 2003; Grady et al. 2004). Our wide-separation companion search (Section 4.2.2) also suggests that the previously identified ϵCA member CXOU J115908.2−781232 is a possible additional companion to HD 104237A. We also flagged HD 104237E as a possible photometric binary, as noted in Section 4.2.1. While stellar components A, D, and E were all resolved within Gaia DR2, B and C were not, most likely being incorporated into the Gaia point-spread function of HD 104237A.

The majority of stars in the HD 104237 system lie near the spatial median of ϵCA, the densest region of ϵCA, and the

system is well within the group's tidal radius (Section 5.2). However, the Gaia DR2 parallaxes of HD 104237D and E place these two stars 6–7 pc closer to Earth than HD 104237A. Indeed, during our wide-separation companion search, HD 104237D+E flagged each other, while HD 104237A only matched (in terms of parallax and proper motion tolerances) with the star CXOU J115908.2−781232. If HD 104237A+E is in fact a bound system, this would imply that the Gaia DR2 parallaxes for components D and E are spurious. On the other hand, as in the case of T Cha and J1155−7919A, the star originally designated T Cha B (Kastner et al. 2012; Kastner 2018), it is possible that the apparent D and E components of the HD 104237 system are in fact merely ϵCA members that are seen in projection near the bright primary star. This would not be surprising, given the system's position near the median *XYZ* of ϵCA. If the potential new components of HD 104237, CXOU J115908.2−781232 and HD 104237Eb, are, in fact, bound to HD 104237A, this could be a seven-star system. Alternatively, the bound components may in fact consist of a triple system comprising HD 104237Ea+Eb+D plus a quadruple system comprising HD 104237A+B+C and CXOU J115908.2−781232. Gaia DR3 should help resolve some of this uncertainty concerning the composition of the HD 104237 system by confirming and/or refining the DR2 parallaxes to its individual components.
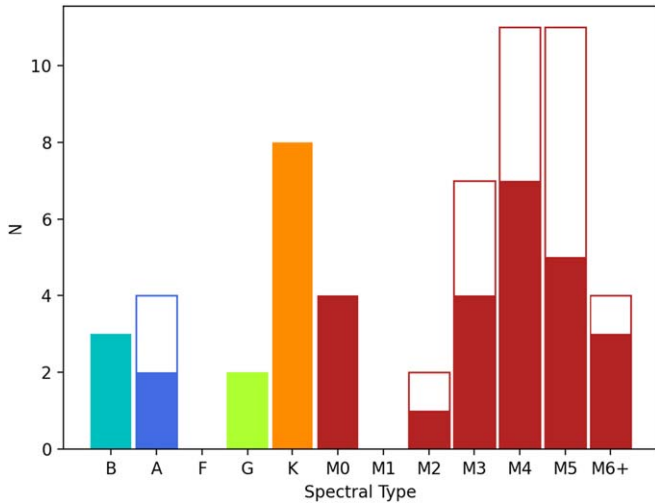
Figure 7. Spectral type histogram compiled from the final ϵCA membership lists (Table 3 and 4). Unfilled portions of the histogram bars indicate provisional members. Non-M spectral types are grouped across subtypes, while the M subtypes are plotted individually. The color scheme follows that of Figure 9 of Lee & Song (2019).

5. Discussion

5.1. Multiplicity Fraction and Spectral Type Distribution

In light of the preceding, we can now revisit the ϵCA multiplicity fraction (MF), or the number of systems consisting of more than one star. Previous to this work, it was found that higher mass stars of ϵCA all have companions, while the lower-mass stars have a low companion frequency (Briceño & Tokovinin 2017). The binary fraction, including suspected binaries, was reported in M+13 as $36^{+10}_{-8}\%$. The MF of our final membership list (Table 3) is 40%, with 12 of 30 systems in multiple systems, which is consistent within the errors with the MF determined by M+13.

We further separate the MF of ϵCA into mass groups, bearing in mind small number statistics. For the population of intermediate-mass (A and B, $n = 5$), solar-type (F, G, and K, $n = 11$), and low-mass (M, $n = 19$) star systems in ϵCA we find MF = 100%, MF = 36%, and MF = 42%, respectively. This can be compared with the MFs of intermediate-mass, solar-type mass, and low-mass stars on the main sequence, for which the MFs are on average MF $\geqslant$ 50%, MF = 44% $\pm$ 2%, and MF = 26% $\pm$ 3%, respectively (Duchêne & Kraus 2013). In contrast, the MF of T associations lies in the range $\sim$66%–75% (Duchêne & Kraus 2013). The MF of ϵCA is hence less than that of T associations and greater than that of MS stars. This is consistent with the $\sim$5 Myr age of ϵCA (Section 5.3), which is intermediate between T associations and the MS field. The ϵCA hence appears to be a key group in which to study the dissolution of young binary systems as T associations evolve toward the field population.

Figure 7 presents the spectral type distribution obtained from our final membership list (Table 3). For purposes of this histogram, K stars of all subtypes are grouped together. The figure demonstrates that the ϵCA spectral type distribution, which peaks at M4, resembles that of the χ^1 For cluster (see Figure 6 in Zuckerman et al. 2019) and other nearby associations like TWA, BPMG, and Columba, many of which have far better statistics (see, e.g., Figure 9 in Lee & Song 2019).
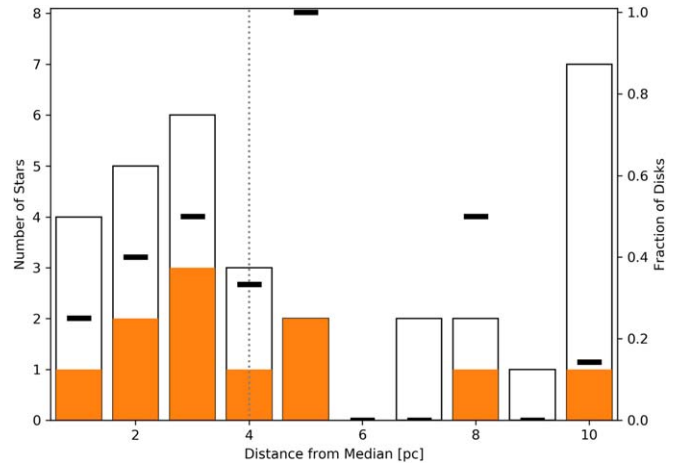

Figure 8. Histogram of the distance from the median XYZ position for the final list of ϵCA members (Table 3). The filled orange bars indicate stars with disks, and the disk fractions are represented as horizontal black lines. The tidal shredding radius (4 pc; Section 5.2) is denoted by a vertical gray dashed line.

5.2. Structure of the Association

With accurate heliocentric positions, we can analyze the structure of the ϵCA NYMG in the Galactic context. Following Zuckerman et al. (2019), the tidal radius of the group can be roughly estimated as $r = R(M_c/3M_g)^{1/3}$ (King 1962), where R is the distance between Earth and the Galactic Center ($\sim$8200 pc), M_c is the mass of the stellar group, and M_g is the Galactic mass interior to the Sun ($\sim$10^{11} $M_\odot$). In order to obtain a rough estimate for M_c, we adopt masses of 3.0, 2.0, 1.0, 0.7, and 0.3 $M_\odot$ for B, A, G, K, and M stars, respectively. We then obtain an estimate for the group mass, based on the spectral types of individual bona fide members of the Association (Table 3), of $M_c \sim 28\ M_\odot$.[6] Adopting this value of M_c, the tidal shredding radius of the group is found to be 4 pc, with a large uncertainty (given the large uncertainties in the estimates of the ϵCA and Galactic masses). Given the estimated group mass and this tidal radius, and assuming (for simplicity) a spherical stellar distribution, the mass density is $\sim$0.13 $M_\odot$ pc^{-3} and the stellar density is $\sim$0.18 pc^{-3}. This mass density is within a factor of 2 of the estimated local Galactic disk density ($\sim 0.1 M_\odot$ pc^{-3}; Mamajek 2016), reflecting the fact that ϵCA is a diffuse association (as opposed to cluster). Inclusion of provisional members would increase the Association mass estimate to $36 M_\odot$ but negligibly change the aforementioned tidal radius and density calculations.

The spatial and kinematic structure of the final membership of the ϵCA is illustrated in Figure 6. The vast majority of group members ($\sim$80%) fall within the tidal shredding radius of the median group XYZ position, shown as the green shaded circle and red cross, respectively. The binaries in the group fall both inside and outside of the central region of the association, with no obvious correlation with position. Figure 8 illustrates the disk fraction versus distance from the median XYZ position of ϵCA. The figure indicates that 9 of the 11 ϵCA systems known to host disks lie within 5 pc of the median position, a volume roughly coincident with that defined by the group's tidal shredding radius; the disk fraction falls from $\sim$50% within 5 pc of the median position to $\sim$15% beyond 5 pc of the median.

---

[6] Note that this estimate ignores the potential contribution to M_c of molecular gas possibly associated with ϵCA—or at least with T Cha—as evidenced by detection of interstellar CO at coincident RV (Sacco et al. 2014).
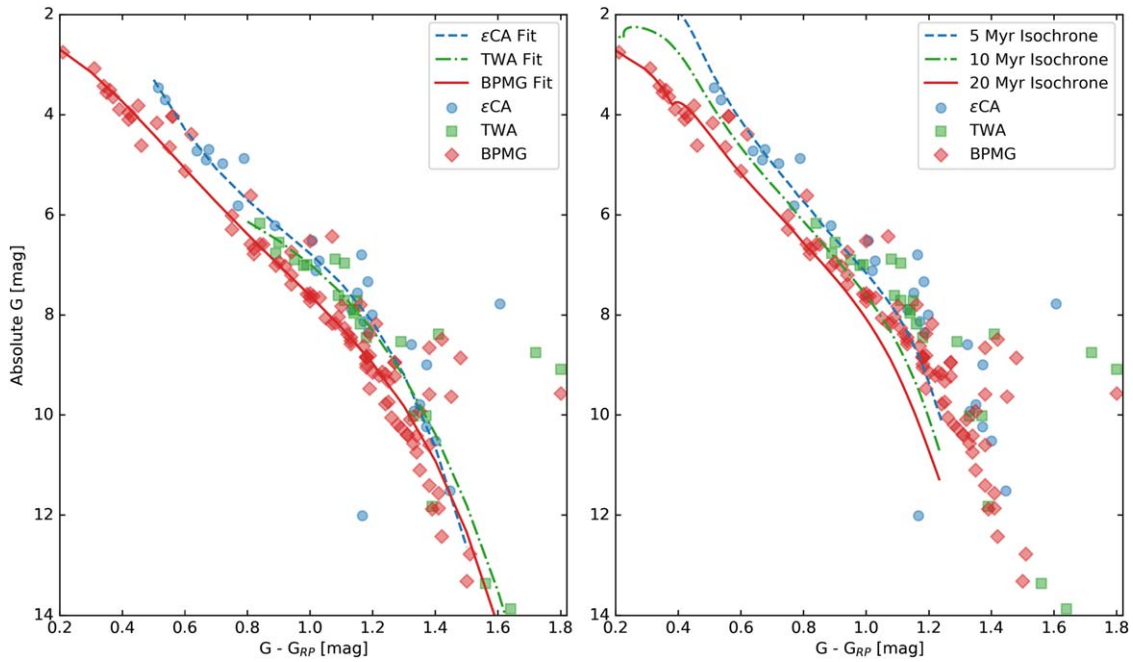
Figure 9. Gaia DR2 CMDs for ϵCA (Table 3; blue circles), the TW Hya Association (green squares), and the β Pic Moving Group (red diamonds), where data for the latter two groups are based on for the membership lists in Lee & Song (2019). In the left panel, the data for the three groups are overlaid with the corresponding empirical isochrones obtained from SLFR analysis (Sections 3.1 and 5.3). In the right panel, the data are overlaid with theoretical isochrones from Tognelli et al. (2018) for ages of 5, 10, and 20 Myr.

This centrally concentrated distribution suggests that stars in the core region of the ϵCA are more likely to retain dusty disks, hinting at the possibility that the nascent planetary systems orbiting stars in this region are subject to more frequent and/or more catastrophic dust-generating collisions. The distribution in Figure 8 stands in contrast to that of the (older) χ^1 For cluster (age ~40 Myr), for which the majority of stars with IR excesses (hence dusty disks) lie in a narrow, spherical annulus just outside the tidal shredding radius of the cluster (Zuckerman et al. 2019). However, as noted by those authors, χ^1 For also represents a particularly striking and unusual case of a large disk frequency in a ~40 Myr old cluster.

5.3. Age of the Association

The SLFR analysis applied to ϵCA (Section 3.1) was additionally performed for two other NYMGs, the TW Hya Association (TWA) and β Pic Moving Group (BPMG). These NYMGs are both slightly older than ϵCA, at 8 Myr (Donaldson et al. 2016) and 24 Myr (Bell et al. 2015), respectively, and hence provide good references for the relative age of ϵCA as determined from their respective SLFR-based empirical isochrones. For our SLFR analysis, we used lists of stars considered bona fide members of each group (Lee & Song 2019), totaling 30 stars for TWA and 113 stars for BPMG.

The empirical isochrones for the three NYMGs are compared in the right panel of Figure 9. With the exception of BPMG, the blue ends of the empirical isochrones are not well fit, due to the small sample sizes in these regions, and are hence not plotted in Figure 9 (and are excluded from this discussion). All three of the empirical isochrones fit their respective NYMG data well in the regions $0.2 \leqslant G - R_p \leqslant 1.2$. In this CMD region, the empirical isochrones show the expected hierarchical pattern—i.e., with ϵCA highest, BMPG lowest, and TWA intermediate between the two—reflecting the relative ages of these three NYMGs. At redder colors, all three groups drop off in population and appear

to display a larger degree of scatter, and hence the empirical isochrones (fourth-order polynomials) do not provide as good a fit in these regions.

Three representative isochrones from Tognelli et al. (2018) are shown in the right panel of Figure 9.[7] While the theoretical isochrones well match the Gaia NYMG data blueward of $G - R_p \sim 0.8$ (apart from the TWA, which lacks stars in this region), these curves fall below the Gaia data at regions redder than $\simeq 0.9$ in $G - R_p$. This divergence between theoretical isochrones and data is commonly observed in Gaia CMDs, as previously noted (Section 3.1), and can likely be ascribed to the high levels of magnetic activity of late K and M stars (e.g., Gagné et al. 2018a).

Based on the close correspondence of the theoretical 5 Myr isochrone and the empirical (SLFR-generated) single-star isochrone in the region $0.5 \leqslant G - R_p \leqslant 1.0$, we estimate an age of 5^{+3}_{-2} Myr for ϵCA, where the range of uncertainty is based on the vertical offset of the 3 and 8 Myr theoretical isochrones in this same domain of $G - R_p$. This is consistent with the age range determined via theoretical isochrone analysis in the (pre-Gaia) M +13 study, i.e., a median of 3–5 $M_\odot$ for lower-mass stars (albeit with somewhat older inferred ages for solar-mass stars), as well as with the age obtained from a reanalysis of the M+13 data by $(3.7^{+4.6}_{-1.4}$ Myr; Schutte et al. 2020). Future age estimates for the ϵCA should be informed by spectroscopic observations designed to confirm the membership status of provisional members (Table 4), a DR3-based search for additional members, and application of isochrones obtained from "magnetic" pre-MS evolution models (e.g., Simon et al. 2019).

---

[7] We found MIST isochrones (Paxton et al. 2011, 2013, 2015; Choi et al. 2016; Dotter 2016) to be indistinguishable from the Tognelli et al. (2018) curves, so only the latter are used as representative of the expected temporal behavior.

Dickson-Vandervelde, Wilson, & Kastner

6. Summary

We have used Gaia DR2 astrometric and photometric data to refine the membership of ϵCA and have thereby established the distance (mean $D = 100.99$ pc, $\sigma_D = 4.62$ pc), age (5^{+3}_{-2} Myr), and spatial and kinematic distributions (Figure 6; Table 7) of the association. We confirm that ϵCA is significantly younger than both the TW Hya Association and β Pic Moving Group (Figure 9) and, hence, that ϵCA represents the youngest NYMG within $\sim$100 pc of Earth. Our analysis includes the determination of an empirical relationship between Gaia $G - G_{RP}$ color and spectral type that should provide an accurate means to determine the spectral subtypes of $\sim$5 Myr old K and M stars from dereddened Gaia photometry.

Our analysis yields a final ϵCA membership list consisting of 36 bona fide members and 20 provisional members (Table 3; Table 4). The provisional members require follow-up study (in particular, RV determinations) in order to confirm their membership status kinematically. These include three new members of the ϵCA that we have identified via a search of Gaia DR2 for wide-separation, comoving companions to previously identified members. One of these newly identified members is either a substellar object or an M star viewed through (and hence highly obscured by) a nearly edge-on circumstellar disk. We identified five photometric binaries among the group members, three of which are new binary-star candidates.

Like other nearby stellar groups, the presently known membership of ϵCA is dominated by M stars, and the spectral type distribution peaks in the mid-M range. The MF of ϵCA (40%) is intermediate between those of the field star population and T associations. We find an overall circumstellar disk fraction of 30% for ϵCA, with the vast majority of disk-bearing stars lying within $\sim$5 pc (Figures 6 and 8).

In providing a well-defined region of *XYZ* and *UVW* space encompassing this NYMG, this work sets the stage for a more complete search of Gaia DR2 (and eventual DR3) data for new members of ϵCA. This work thereby provides the framework for future investigations of the initial mass function as well as multiplicity and disk fractions of ϵCA.

ORCID iDs

Emily C. Wilson ● https://orcid.org/0000-0002-3947-5586
Joel H. Kastner ● https://orcid.org/0000-0002-3138-8250

References

Alencar, S. H. P., Teixeira, P. S., Guimarães, M. M., et al. 2010, A&A, 519, A88
Bell, C. P. M., Mamajek, E. E., & Naylor, T. 2015, MNRAS, 454, 593
Belokurov, V., Penoyre, Z., Oh, S., et al. 2020, MNRAS, 496, 1922
Briceño, C., & Tokovinin, A. 2017, AJ, 154, 195
Cardelli, J. A., Clayton, G. C., & Mathis, J. S. 1989, ApJ, 345, 245
Choi, J., Dotter, A., Conroy, C., et al. 2016, ApJ, 823, 102
Desidera, S., Covino, E., Messina, S., et al. 2015, A&A, 573, A126
Dickson-Vandervelde, D. A., Wilson, E. C., & Kastner, J. H. 2020, RNAAS, 4, 25
Donaldson, J. K., Weinberger, A. J., Gagné, J., et al. 2016, ApJ, 833, 95
Dotter, A. 2016, ApJS, 222, 8
Duchêne, G., & Kraus, A. 2013, ARA&A, 51, 269
Fang, M., van Boekel, R., Bouwman, J., et al. 2013, A&A, 549, A15
Feigelson, E. D., Lawson, W. A., & Garmire, G. P. 2003, ApJ, 599, 1207
Gagné, J., & Faherty, J. K. 2018, ApJ, 862, 138
Gagné, J., Faherty, J. K., & Mamajek, E. E. 2018a, ApJ, 865, 136
Gagné, J., Gonzales, E. C., & Faherty, J. K. 2018b, RNAAS, 2, 17
Gagné, J., Mamajek, E. E., Malo, L., et al. 2018c, ApJ, 856, 23
Gaia Collaboration, Brown, A. G. A., Vallenari, A., et al. 2018, A&A, 616, A1
Gaia Collaboration, Prusti, T., de Bruijne, J. H. J., et al. 2016, A&A, 595, A1
Gontcharov, G. A. 2006, AstL, 32, 759
Grady, C. A., Woodgate, B., Torres, C. A. O., et al. 2004, ApJ, 608, 809
Guenther, E. W., Esposito, M., Mundt, R., et al. 2007, A&A, 467, 1147
Hales, A. S., De Gregorio-Monsalvo, I., Montesinos, B., et al. 2014, AJ, 148, 47
Hendler, N. P., Pinilla, P., Pascucci, I., et al. 2018, MNRAS, 475, L62
Kastner, J., Allers, K., Bowler, B., et al. 2019, BAAS, 51, 294
Kastner, J. H. 2018, RNAAS, 2, 137
Kastner, J. H., Hily-Blant, P., Sacco, G. G., Forveille, T., & Zuckerman, B. 2010, ApJL, 723, L248
Kastner, J. H., Thompson, E. A., Montez, R., et al. 2012, ApJL, 747, L23
King, I. 1962, AJ, 67, 471
Köhler, R. 2001, AJ, 122, 3325
Kordopatis, G., Gilmore, G., Steinmetz, M., et al. 2013, AJ, 146, 134
Lee, J., & Song, I. 2019, MNRAS, 486, 3434
Lindegren, L. 2018, Re-normalising the Astrometricchi-square in Gaia DR2, Rep. GAIA-C3-TN-LU-LL-124-01, http://www.rssd.esa.int/doc_fetch.php?id=3757412
Lindegren, L., Hernández, J., Bombrun, A., et al. 2018, A&A, 616, A2
Lopez Martí, B., Jimenez Esteban, F., Bayo, A., et al. 2013, A&A, 551, A46
Luhman, K. L. 2004, ApJ, 616, 1033
Malo, L., Artigau, É., Doyon, R., et al. 2014, ApJ, 788, 81
Mamajek, E. E. 2016, in IAU Symp. 314, Young Stars & Planets Near the Sun, ed. J. H. Kastner, B. Stelzer, & S. A. Metchev (Cambridge: Cambridge Univ. Press), 21
Mamajek, E. E., Lawson, W. A., & Feigelson, E. D. 2000, ApJ, 544, 356
Murphy, S. J., Lawson, W. A., & Bessell, M. S. 2013, MNRAS, 435, 1325
Olofsson, J., Benisty, M., Le Bouquin, J. B., et al. 2013, A&A, 552, A4
Paxton, B., Bildsten, L., Dotter, A., et al. 2011, ApJS, 192, 3
Paxton, B., Cantiello, M., Arras, P., et al. 2013, ApJS, 208, 4
Paxton, B., Marchant, P., Schwab, J., et al. 2015, ApJS, 220, 15
Pecaut, M. J., & Mamajek, E. E. 2013, ApJS, 208, 9
Phillips, C. L., Bowler, B. P., Mace, G., Liu, M. C., & Sokal, K. 2020, ApJ, 896, 173
Sacco, G. G., Kastner, J. H., Forveille, T., et al. 2014, A&A, 561, A42
Schisano, E., Covino, E., Alcalá, J. M., et al. 2009, A&A, 501, 1013
Schneider, A. C., Shkolnik, E. L., Allers, K. N., et al. 2019, AJ, 157, 234
Schutte, M. C., Lawson, K. D., Wisniewski, J. P., et al. 2020, AJ, 160, 156
Simon, M., Guilloteau, S., Beck, T. L., et al. 2019, ApJ, 884, 42
Skrutskie, M. F., Cutri, R. M., Stiening, R., et al. 2006, AJ, 131, 1163
Terranegra, L., Morale, F., Spagna, A., Massone, G., & Lattanzi, M. G. 1999, A&A, 341, L79
Testa, P., Huenemoerder, D. P., Schulz, N. S., & Ishibashi, K. 2008, ApJ, 687, 579
Tognelli, E., Prada Moroni, P. G., & Degl'Innocenti, S. 2018, MNRAS, 476, 27
Torres, C. A. O., Quast, G. R., da Silva, L., et al. 2006, A&A, 460, 695
Torres, C. A. O., Quast, G. R., Melo, C. H. F., & Sterzik, M. F. 2008, in Handbook of Star Forming Regions, Vol. II, ed. B. Reipurth (San Francisco, CA: ASP), 757
Wright, N. J., & Mamajek, E. E. 2018, MNRAS, 476, 381
Zuckerman, B., Klein, B., & Kastner, J. 2019, ApJ, 887, 87